

# Driver-Automation Cooperation Oriented Approach for Shared Control of Lane Keeping Assist Systems

Chouki Sentouh, Anh-Tu Nguyen<sup>✉</sup>, Mohamed Amir Benloucif, and Jean-Christophe Popieul

**Abstract**—This paper presents a novel shared control concept for lane keeping assist (LKA) systems of intelligent vehicles. The core idea is to combine *system perception* with *robust control* so that the proposed strategy can successfully share the control authority between human drivers and the LKA system. This shared control strategy is composed of two parts, namely an operational part and a tactical part. Two local optimal-based controllers with two predefined objectives (i.e., lane keeping and conflict management) are designed in the operational part. The control supervisor in the tactical part aims to provide a decision-making signal which allows for a smooth transition between two local controllers. The control design is based on a human-in-the-loop vehicle system to improve the mutual driver-automation understanding, thus reducing or avoiding the conflict. The closed-loop stability of the whole driver-vehicle system can be rigorously guaranteed using the Lyapunov stability argument. In particular, the control design is formulated as an LMI optimization which can be easily solved with numerical solvers. The effectiveness of the proposed shared control method is clearly demonstrated through various hardware experiments with human drivers.

**Index Terms**—Advanced driver assistance systems (ADASs), control authority transition, human-in-the-loop control, linear matrix inequality (LMI), shared control, vehicle control.

## I. INTRODUCTION

DIVING is a dangerous activity, and the damages caused by road accidents have serious consequences for individuals and the society [1], [2]. The failure of human driver's performance (e.g., due to inattention, drowsiness, and illness) remains one of the most important causes of accidents [1], [3]. Therefore, advanced driver assistance systems (ADASs) have become the focus of intensive investigations conducted in both

Manuscript received October 5, 2016; revised September 12, 2017; accepted May 23, 2018. Manuscript received in final form May 28, 2018. This work was supported in part by the AutoConduct Project through the Agence Nationale de la Recherche under Grant ANR-16-CE22-0007, in part by the ELSAT2020 Project, in part by the International Campus on Safety and Intermodality in Transportation, in part by the Hauts-de-France Region, in part by the European Community, in part by the Regional Delegation for Research and Technology, in part by the Ministry of Higher Education and Research, and in part by the French National Center for Scientific Research. Recommended by Associate Editor M. Tanelli. (*Corresponding author: Anh-Tu Nguyen*.)

The authors are with the Laboratoire d'Automatique, de Mécanique et d'Informatique industrielles et Humaines (LAMIH UMR CNRS 8201), Université Polytechnique Hauts-de-France, 59300 Valenciennes, France (e-mail: nguyen.tranhantru@gmail.com).

Color versions of one or more of the figures in this paper are available online at <http://ieeexplore.ieee.org>.

Digital Object Identifier 10.1109/TCST.2018.2842211

academic and industry settings [4]–[6]. These systems aim to assist drivers by enhancing their sensing ability, warning in the case of human errors, and reducing the driver's workload [5]. They adopt multiple forms and can be categorized according to the level of automation, the interaction with human drivers, and so forth [1], [7]. Although technological advances have been significantly made to improve the performance of ADAS, the control issue of active safety systems being able to share the driving responsibility with human drivers still remains challenging [5], [8]–[10]. Most of existing works have mainly focused on the automatic control of the ADAS without paying special attention on the driver's control actions [6]. However, these latter can be appeared as a destabilizing part of the vehicle system [11]. Note also that the integration of a new assistance system into the vehicle could have negative impacts on driver's safety and comfort unless it is incorporated to work *jointly* with human drivers [9].

This paper is concerned with the shared steering control of a lane keeping assist (LKA) system in highway driving conditions. Using a vision system to track the road markings, such an assistance system can estimate the vehicle lateral position with respect to the road centerline; at the same time, it can *continuously* interact with human drivers for driving automation. The concept of driver-automation shared control means that both driving actors should have *simultaneously* the vehicle control via the steering wheel so that the human driver may express his/her control intentions in a way that either overrides the automation or conforms to it [9], [12], [13]. This approach has demonstrated many benefits like improving the driving performance and reducing the driver's control effort [13]. Note that the need for an active coordination of control authority between human drivers and the automation in the control framework of LKA systems has been recognized in [7], [9], and [14]. However, up to now, shared steering control which can *adaptively* modify the control authority allocation between human drivers and the LKA system according to the driving conditions is still open due to the complex human-machine interaction involved in the design procedure.

A steering wheel angle has been considered as the control input in most of existing works, for instance [15]–[18]. In general, the resulting control methods offer a good robustness performance, because the nonlinearities of steering system can be easily compensated [16], [19], [20]. However, these

methods do not allow for a possible intervention of driver's actions which are considered as system disturbances. Therefore, *shared driving* concept cannot be achieved with such controllers. In [19], a combined automatic lane-keeping and driver's steering using a two-degrees-of-freedom control strategy has been proposed. There is no need for ON/OFF switching strategy, and the control loop is always active to guarantee either manual or automatic steering mode. However, this control strategy can only guarantee either manual or automatic steering modes without any possibility for driver-automation cooperation. Shared control approaches have been developed in the framework of intelligent vehicles [8], [10], [21]. In these works, the control design is based on a simple static lane-keeping driver model [10], [21], or the degree of cooperation is quantified by quadratic optimization criteria [8]. Note that no real-time information on driver's behaviors under *unpredictable* driving environment has been considered in [8]. Hence, the conflict issue between human drivers and the LKA system seems hard to be solved for general situations. Using the steer-by-wire technology, a model predictive control framework for shared control has been recently presented in [22] where the control objective of matching the driver's steering angle is opposed to other ones, such as vehicle stability and obstacle avoidance. In particular, the final control authority is always given to the LKA system and the driver cannot overrule it.

In order to overcome the above-mentioned drawbacks of existing shared control methods for LKA systems, we propose to take into account in the control design not only the driver's behaviors (via modeling and measurements) but also the vehicle environment perception. As will be shown, an appropriate integration of such information is crucial to deal with the challenging human-machine conflict issue. Inspired by the concept of *multiple controller switching* [23], the new shared control method is able to meet several conflicting specifications, namely vehicle stability and tracking performance, damping compensation, and conflict minimization. To achieve this goal, the proposed shared control paradigm, called *two-level cooperative control scheme*, is composed of two hierarchical parts: a *tactical* part and an *operational* part. The control supervisor in the tactical part aims at orchestrating a smooth control authority transition between human drivers and the LKA system. For the supervisor design, we fully exploit the information from: 1) the driver monitoring system (DMS) (for driver state evaluation) [24], [25] and 2) the vehicle vision system (for environment perception and risk evaluation). The operational part aims to compute directly the assistance actions of the LKA system. This part is composed of two local optimal-based controllers which are linked each other via a smooth transition signal provided by the tactical part. Based on a human-in-the-loop vehicle (HiLV) model, the feedback gains of both controllers are designed using the Lyapunov stability argument. This not only guarantees rigorously the closed-loop stability but also improves the mutual understanding between human drivers and the LKA system. In particular, the control design is cast as a linear matrix inequality (LMI) optimization which is easily solved with numerical solvers [26].

TABLE I  
VEHICLE NOMENCLATURE

Notation	Description
$m$	mass of vehicle [kg]
$C_f/C_r$	cornering stiffness of the front/rear tires [N/rad]
$I_z$	moment inertia about the yaw axis [ $\text{kgm}^2$ ]
$l_f/l_r$	distances of the front/rear tire from CG [m]
$l_w$	lateral wind force impact distance [m]
$l_p$	look-ahead distance [m]
$f_w$	lateral wind force [N]
$v_x/v_y$	vehicle longitudinal/lateral speed [m/s]
$\beta$	vehicle sideslip angle [rad]
$r$	vehicle yaw rate [rad/s]
$\psi_L$	relative yaw angle [rad]
$y_L$	lateral offset from the centerline [m]
$\delta_d$	steering wheel angle at the column system [rad]
$J_s$	moment of inertia of the steering system [ $\text{kgm}^2$ ]
$B_s$	damping coefficient of the steering system [Nm/rad/s]
$R_s$	reduction ratio of the steering system [-]
$\eta_t$	width of the tire contact [m]
$T_a/T_d/T_s$	assistance/driver/self-aligning torque [Nm]

The novel feature of the proposed shared control method relies on the combination of *system perception* (from the tactical part) and *robust control approach* (from the operational part). This outstanding feature offers an effective solution for the shared steering control issue. As a consequence, the developed LKA system can *adaptively* assist human drivers according to their real-time driving activities and the driving risk evaluation to avoid/minimize the driver-automation conflict. The effectiveness of the proposed method has been clearly demonstrated through various experimental tests conducted on the SHERPA dynamic driving simulator with human drivers.

This paper is organized as follows. Section II discusses on the modeling and the experimental validation of an HiLV model used for the control design. The proposed shared control method is detailed in Section III. Experimental results with various driving scenarios and several human drivers are shown in Section V. Section VI provides some concluding remarks.

*Notation:* For matrix  $M$ ,  $M^\top$  denotes its transpose. For square matrix  $X$ ,  $X > 0$  means that  $X$  is positive definite, and  $\text{He}(X) = X + X^\top$ .  $I$  denotes the identity matrix of appropriate dimensions. Given square matrices  $X_1$  and  $X_2$ , we denote  $\text{diag}(X_1, X_2)$  the diagonal block matrix with  $X_i$  on the  $i$ th diagonal entry. The symbol  $*$  stands for matrix blocks that can be deduced by symmetry; for in-line expressions, it indicates the transpose of the terms on its left side. Arguments will be omitted when their meaning is clear.

## II. VEHICLE AND DRIVER MODELING

This section presents briefly the modeling of the road-vehicle system and the driver's behaviors for shared lateral control purposes. The vehicle notation is given in Table I.

### A. Road-Vehicle Control-Based Model

In this paper, the vehicle lateral dynamics is represented by the well-known bicycle model [19], [27] (see Fig. 1). This model is directly derived from the nonlinear four-wheel vehicle system [27] while assuming: 1) the dynamics of the

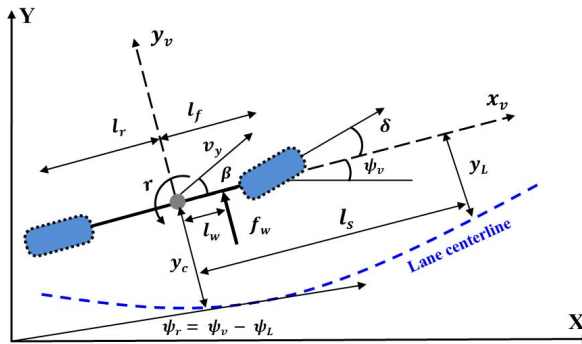


Fig. 1. Lateral vehicle behavior modeling.

vehicle speed  $v_x$  and the aerodynamic forces are neglected; 2) the lateral tire forces are proportional to the slip angles of each axle; and 3) the small angle assumption is considered. Note that these assumptions are appropriate for highway driving under mild acceleration conditions and have been widely adopted for lateral control [3], [19], [27] and shared lateral control [8], [21]. The vehicle lateral dynamics can be given by

$$\begin{bmatrix} \dot{\beta} \\ \dot{r} \end{bmatrix} = \begin{bmatrix} a_{11} & a_{12} \\ a_{21} & a_{22} \end{bmatrix} \begin{bmatrix} \beta \\ r \end{bmatrix} + \begin{bmatrix} b_1 \\ b_2 \end{bmatrix} \delta + \begin{bmatrix} e_1 \\ e_2 \end{bmatrix} f_w \quad (1)$$

where  $\beta$  is the sideslip angle at the center of gravity (CG),  $r$  is the yaw rate, and  $f_w$  denotes the lateral wind force. The matrix elements in (1) are defined as follows:

$$\begin{aligned} a_{11} &= -\frac{2(C_r + C_f)}{mv_x}, \quad a_{12} = \frac{2(l_r C_r - l_f C_f)}{mv_x^2} - 1 \\ a_{21} &= \frac{2(l_r C_r - l_f C_f)}{I_z}, \quad a_{22} = -\frac{2(l_r^2 C_r + l_f^2 C_f)}{I_z v_x} \\ b_1 &= \frac{2C_f}{mv_x}, \quad b_2 = \frac{2l_f C_f}{I_z}, \quad e_1 = \frac{1}{mv_x}, \quad e_2 = \frac{l_w}{I_z}. \end{aligned}$$

*Remark 1:* Note that besides the wind effects, other sources of disturbances affecting the vehicle dynamics can be encountered in practice, such as the road crown (sloping to one side) or the superelevation (banking in turns). However, these disturbances can be dealt with by the proposed robust controller in the same way as the lateral wind force.

For lane keeping control, the vehicle positioning on the road must be studied (see Fig. 1). To this end, the following dynamics of two supplementary variables provided by the vehicle vision system, namely lateral deviation error  $y_L$  and heading error  $\psi_L$ , are incorporated into (1):

$$\dot{y}_L = \beta v_x + l_p r + \psi_L v_x, \quad \dot{\psi}_L = r - \rho_r v_x \quad (2)$$

where  $\rho_r$  is the road curvature defined as  $\rho_r = 1/R_r$ , with  $R_r$  the curvature radius. Note that the above-mentioned dynamics of  $y_L$  and  $\psi_L$  have been considered in various control contexts of intelligent vehicles with experimental validations [3], [8], [21].

To quantify the driver's feeling with respect to the feedback torque provided by the LKA system, the following steering system is also integrated into vehicle system [3]:

$$J_s \ddot{\delta}_d + B_u \dot{\delta}_d + K_s \delta_d = T_d + T_a - T_s \quad (3)$$

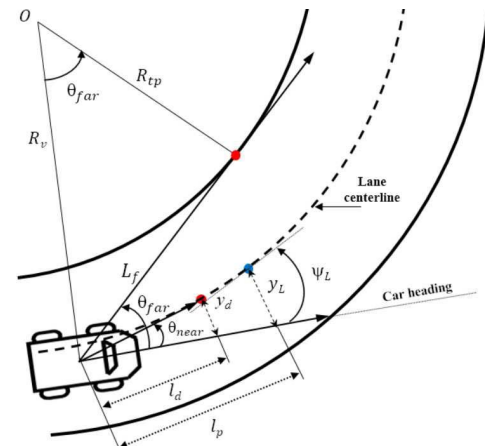


Fig. 2. Visual angles for anticipatory and compensatory driving tasks.

where the expression of the self-aligning torque is given by

$$T_s = -\frac{2C_f \eta_t}{R_s} \beta - \frac{2l_f C_f \eta_t}{R_s v_x} r + \frac{2C_f \eta_t}{R_s^2} \delta_d.$$

From (1)–(3), the road-vehicle model used for control purposes can be represented in the following form:

$$\dot{x}_v = A_v x_v + B_{vu} u_v + B_{vw} w \quad (4)$$

where  $x_v = [\beta \ r \ \psi_L \ y_L \ \delta_d \ \dot{\delta}_d]^T$  is the vehicle state,  $w = [f_w \ \rho_r]^T$  is the disturbance vector, and the control input  $u_v$  is composed by the assistance and driver torques  $u_v = T_a + T_d$ . The system matrices of (4) are given by

$$A_v = \begin{bmatrix} a_{11} & a_{12} & 0 & 0 & b_1/R_s & 0 \\ a_{21} & a_{22} & 0 & 0 & b_2/R_s & 0 \\ 0 & 1 & 0 & 0 & 0 & 0 \\ v_x & l_p & v_x & 0 & 0 & 0 \\ 0 & 0 & 0 & 0 & 0 & 1 \\ a_{61} & a_{62} & 0 & 0 & a_{65} & a_{66} \end{bmatrix}, \quad B_{vu} = \begin{bmatrix} 0 \\ 0 \\ 0 \\ 0 \\ 0 \\ 1/J_s \end{bmatrix}$$

$$B_{vw}^\top = \begin{bmatrix} e_1 & e_2 & 0 & 0 & 0 & 0 \\ 0 & 0 & -v_x & 0 & 0 & 0 \end{bmatrix}, \quad a_{61} = \frac{2C_f \eta_t}{R_s J_s}$$

$$a_{62} = \frac{2C_f l_f \eta_t}{R_s v_x J_s}, \quad a_{65} = \frac{-2C_f \eta_t}{R_s^2 J_s}, \quad a_{66} = \frac{-B_u}{J_s}.$$

### B. Simplified Driver Model

It has been shown that for driving tasks, the driver is guided on the road by looking at two specific points called *near point* and *far point* [28]–[30] (see Fig. 2). The *near point* corresponding to the lane centerline at a short distance ahead of the vehicle, which represents the perception of the midposition between both the lane edges. The driver tracks the *far point* when negotiating bends. These points can be characterized by two visual angles  $\theta_{near}$  and  $\theta_{far}$  which represent, respectively, the driver's *compensatory* and *anticipatory* behaviors [30]. Several two-level driver models (i.e. using both  $\theta_{near}$  and  $\theta_{far}$ ) have been derived and their effectiveness has also been demonstrated by behavioral studies [29]–[33]. In particular, based on driving simulator experiments performed with several participants, Mars *et al.* [31] have concluded that a two-level

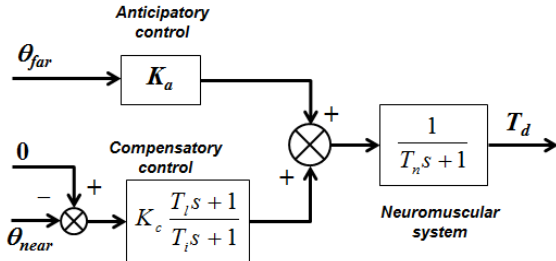


Fig. 3. Block diagram of the two-level driver model.

driver model can be used to reproduce driver's behaviors, and this kind of model is appropriate for the purposes of shared steering control.

A time-delay-based driver model using both visual and kinesthetic perceptions has been well established in [34]. However, this model would be too complex for a possible integration of driver's behaviors into the control design procedure. In what follows, a simplified version of this two-level driver model will be used for control purposes. The block diagram of the two-point visual anticipatory and compensatory driver model considered in this paper is depicted in Fig. 3, and the corresponding system dynamics is given by

$$\dot{x}_d = A_d x_d + B_d u_d, \quad y_d = C_d x_d \quad (5)$$

where the state vector is defined as  $x_d = [x_{d1} \ x_{d2}]^\top$ . The state  $x_{d1}$  is related to the compensatory control block in Fig. 3. This internal state can be interpreted as the driver's perception of the steering wheel correction to be done in a near future by considering the variation of the *near* visual angle  $\theta_{\text{near}}$ . The second state  $x_{d2}$  is the driver torque, i.e.,  $x_{d2} = T_d$ . The input vector  $u_d = [\theta_{\text{near}} \ \theta_{\text{far}}]^\top$  of (5) is detailed later, and the output is  $y_d = T_d$ . The system matrices in (5) are defined as

$$A_d = \begin{bmatrix} -\frac{1}{T_i} & 0 \\ \frac{1}{T_n T_i} - \frac{1}{T_n} & 0 \end{bmatrix}, \quad B_d = \begin{bmatrix} \frac{(T_l - T_i) K_c}{T_i} & 0 \\ -\frac{T_l K_c}{T_i T_n} & \frac{K_a}{T_n} \end{bmatrix} \quad (6)$$

where  $T_l$  and  $T_i$  are, respectively, the lead and lag time constants of the compensatory control block in Fig. 3. The driver's neuromuscular lag time constant is denoted by  $T_n$ . The gains  $K_a$  and  $K_c$  represent, respectively, the visual *anticipatory* control and the visual *compensatory* control. The details on the simplified driver model (5) and the physical interpretation of its parameters in (6) can be found in [34].

*Remark 2:* Thanks to its capacity to integrate both *anticipatory* and *compensatory* control features, the driver model [see (5) and (6)] is able to reproduce the steering behaviors of human drivers in normal driving conditions (such as highway driving) despite the variation of vehicle speed (see [35] for more details). Note that a similar driver model has also been employed in [8] for another shared control context with experimental validation. However, for more aggressive driving situations in rural and extra-urban areas, further studies on the driver modeling would be required.

### C. Human-in-the-Loop Vehicle Model

The HiLV model is obtained by incorporating (5) into (4). To do that, explicit expressions of  $\theta_{\text{near}}$  and  $\theta_{\text{far}}$  are required. The near visual angle can be expressed by

$$\theta_{\text{near}} = y_d / l_d, \quad l_d = v_x T_p \quad (7)$$

where  $l_d$  is the look-ahead distance to the *near point* and  $T_p$  is the driver preview time. The lateral deviation error  $y_d$  at the look-ahead distance  $l_d$  is given by

$$y_d = y_L + (l_d - l_p) \psi_L. \quad (8)$$

It follows easily from (7) and (8) that:

$$\theta_{\text{near}} = \frac{y_L}{v_x T_p} + \left(1 - \frac{l_p}{v_x T_p}\right) \psi_L. \quad (9)$$

The second input  $\theta_{\text{far}}$  of (5) represents the angle between the vehicle heading direction and the tangent point. When the driver tracks the *far point* at a distance  $L_f$ , the road curvature predicted by the driver is given by

$$\rho_{\text{tp}} = r/v_x + L_f \dot{r}/v_x^2$$

where the yaw acceleration  $\dot{r}$  is expressed as follows:

$$\dot{r} = a_{21}\beta + a_{22}r + b_2\delta_d.$$

At the tangent point  $\rho_{\text{tp}} = 1/R_{\text{tp}}$ , one can be approximated as  $\theta_{\text{far}} = L_f/R_{\text{tp}}$  (see Fig. 2). Then, it follows that:

$$\theta_{\text{far}} = \theta_1\beta + \theta_2r + \theta_3\delta_d \quad (10)$$

where  $\theta_1 = \tau_a^2 a_{21}$ ,  $\theta_2 = \tau_a + \tau_a^2 a_{22}$ , and  $\theta_3 = \tau_a^2 b_2/R_s$ . Note that the time to tangent point<sup>1</sup>  $\tau_a = L_f/v_x$  represents the driver's anticipatory time with respect to the tangent point.

It follows from (9) and (10) that:

$$u_d = [\theta_{\text{near}} \ \theta_{\text{far}}]^\top = C x_v$$

$$C = \begin{bmatrix} 0 & 0 & 1 - \frac{l_p}{v_x T_p} & \frac{1}{v_x T_p} & 0 & 0 \\ \theta_1 & \theta_2 & 0 & 0 & \theta_3 & 0 \end{bmatrix}. \quad (11)$$

From (4), (5), (9), and (10), the control-based HiLV model can be rewritten in the following form:

$$\dot{x} = Ax + B_u u + B_w w \quad (12)$$

where the augmented state vector and the control input are, respectively,  $x = [x_v \ x_d]^\top$  and  $u = T_a$ . The system matrices of (12) are given by

$$A = \begin{bmatrix} A_v & B_v C_d \\ B_d C & A_d \end{bmatrix}, \quad B_u = \begin{bmatrix} B_v \\ 0 \end{bmatrix}, \quad B_w = \begin{bmatrix} B_{vw} \\ 0 \end{bmatrix}.$$

Note that the integration of the driver model (5) into the road-vehicle system (4) allows for a possible consideration of some *a priori* information on the driver's driving style, such as the preview time  $T_p$  and the time to tangent point  $\tau_a$ . This consideration is particularly interesting with respect to the human-machine cooperation issue from the point of view of the automatic control design. Indeed, the resulting controller will be able to guarantee a desired driving task without rejecting the driver actions, thus the conflict issue is effectively managed.

<sup>1</sup>When the vehicle is on a straight road section,  $L_f$  is large and  $R_{\text{tp}} \rightarrow \infty$ , then the *far* visual angle is zero. During the curve negotiation,  $L_f$  becomes constant according to the radius of road curvature.

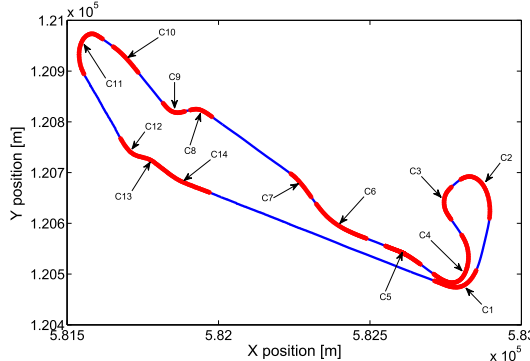


Fig. 4. Satory test track with various levels of road curvature.

#### D. Driver-Vehicle Model Validation

In the sequel, some highlights on the identification of the driver model (5) and the real-time validation of the HiLV system are given. The identification is performed in two phases for simplicity as in [34]. Since  $\tau_a$  appears independently in (10), the first phase is thus to determine the value of  $\tau_a$  from the vehicle data  $\beta$ ,  $r$ ,  $\delta_d$ , and  $\theta_{far}$  using the well-known least squares method. Then, in the second phase, other driver parameters are identified with the prediction error method [36]. For that, the driver model (5) is rewritten as follows:

$$\dot{x}_d = A_d x_d + \tilde{B}_d \tilde{u}_d, \quad \tilde{u}_d = [\psi_L \quad y_L \quad \theta_{far}]^\top$$

where

$$\tilde{B}_d = \begin{bmatrix} \frac{(T_l - T_i)K_c}{T_i} \left(1 - \frac{l_p}{v_x T_p}\right) & \frac{(T_l - T_i)K_c}{T_i v_x T_p} & 0 \\ \frac{-T_l K_c}{T_i T_n} \left(1 - \frac{l_p}{v_x T_p}\right) & \frac{-T_l K_c}{T_i T_n v_x T_p} & \frac{K_a}{T_n} \end{bmatrix}.$$

The parameter vector  $\varpi = [T_l \quad T_i \quad K_a \quad K_c \quad T_n \quad T_p]^\top$  of the driver model can be identified using the command *pem* in the MATLAB *system identification* toolbox.

The identification of the driver parameters has been done with the data of nine participants who were invited to drive the SHERPA simulator (see Section V) on the Satory test track (about 2.3 km long) depicted in Fig. 4 with a fixed speed  $v_x = 20$  [m/s], i.e., the nominal speed of (4). This real-world test track is decomposed into 14 curves of radius ranging from 50 to 500 m which provides rich input signals for the identification. The identification results for the considered set of drivers are given in Table II. We can observe that the driver parameters for nine participants are quite similar with an average fit ratio of 85%. The same remarks can be made for the identification results obtained with  $v_x = 15$  [m/s] and  $v_x = 25$  [m/s], which are not shown here for brevity. For control design, the average values of driver parameters of nine participants will be used as the nominal ones.

Fig. 5 shows the comparison of system responses<sup>2</sup> between the results obtained with the SHERPA simulator and the models given in (4), (5), (9), and (10) for a variable speed profile and a new driver who is not in the set of nine

<sup>2</sup>For brevity, we provide only some significative variables representing both vehicle response and driver's behaviors (i.e.,  $\theta_{near}$  and  $\theta_{far}$ ) in Fig. 5.

TABLE II  
IDENTIFICATION RESULTS OF DRIVER PARAMETERS

Param.	$T_l$	$T_i$	$K_a$	$K_c$	$T_n$	$T_p$	$\tau_a$	Fit %
Driver 1	2.31	0.12	16.38	7.85	0.1	0.81	1.06	86.22
Driver 2	1.20	0.11	16.09	6.43	0.09	0.90	1.02	76.38
Driver 3	1.51	0.15	15.75	8.57	0.12	0.89	1.10	89.85
Driver 4	1.39	0.33	15.51	5.87	0.11	0.62	0.98	86.81
Driver 5	1.93	0.21	15.44	7.21	0.12	0.72	0.98	86.38
Driver 6	1.69	0.24	14.67	5.61	0.11	0.84	1.19	90.56
Driver 7	1.67	0.17	15.04	6.15	0.09	0.66	1.02	85.22
Driver 8	1.17	0.18	15.98	5.79	0.12	0.79	1.12	90.38
Driver 9	1.27	0.14	16.45	8.03	0.11	0.85	0.99	84.53
Average	1.57	0.18	15.70	6.83	0.11	0.79	1.05	86.26

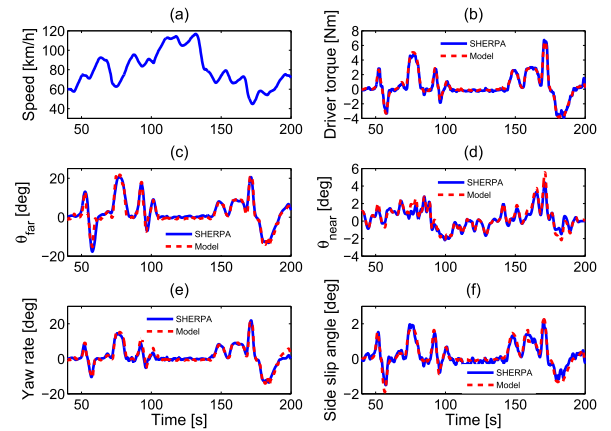


Fig. 5. Experimental validation of driver-vehicle model using Satory test track with variable vehicle speed. Comparison of vehicle responses between SHERPA data (solid line) and HiLV model (12) (dashed line). (a) Vehicle speed. (b) Driver torque with model fit = 85%. (c) Far angle with model fit = 72%. (d) Near angle with model fit = 71%. (e) Yaw rate with model fit = 75%. (f) Sideslip angle with model fit = 68%.

participants for identification. To cover the most significative road curvatures, the corresponding driving scenario used for this validation starts at the beginning of the curve C8 and stops at the end of the curve C4 of the Satory test track in Fig. 4. Observe that the responses of (4), (5), (9), and (10) are highly close to the behaviors of the SHERPA simulator. Therefore, the HiLV model (12) can be clearly exploited for control purposes.

### III. COOPERATIVE CONTROL STRATEGY AND SUPERVISOR DESIGN FOR SHARED CONTROL AUTHORITY

This section provides a description on the proposed cooperative strategy for shared lateral control. To this end, the control problem is first formulated. Some details on the design of the control supervisor will also be discussed.

#### A. Problem Statement and Control Goals

We propose here a novel shared control strategy for an LKA system with the following closed-loop specifications.

- (i) *Stability and tracking performance.* The controller must guarantee the closed-loop stability of the HiLV system while minimizing the lane tracking error.

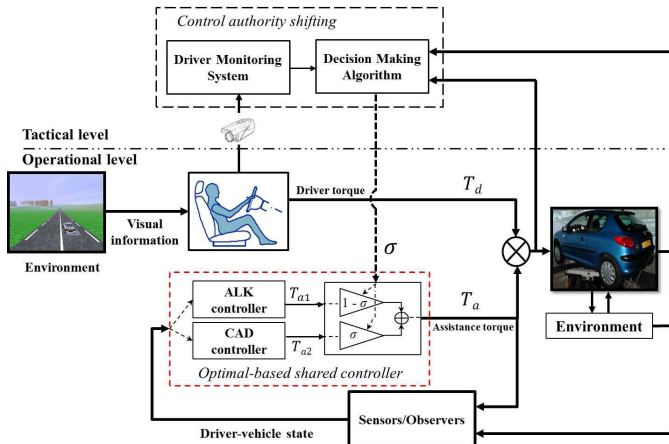


Fig. 6. Block diagram of the proposed two-level cooperative control scheme.

- (ii) *Damping compensation*. When the driver releases the steering wheel without applying any torque, the vibration in the resonance response of vehicle may occur. Then, the controller must be capable of attenuating this vibration effect to improve driving comfort.
- (iii) *Conflict minimization*. The LKA system can share the control authority with human drivers according to their real-time driving activity to manage the conflict issue.

Since the above-mentioned requirements are conflicting, the use of a single linear time-invariant controller could be unsuitable. To overcome that, a new control strategy inspired by the concept of *multiple controller switching* [23] is proposed. Besides performance improvement, this concept provides also an effective control mechanism to deal with complex systems subject to modeling uncertainty [37], such as the HiLV model (12). For its realization, we propose a two-level cooperative control strategy whose structure is depicted in Fig. 6. This control strategy is composed of two following levels.

1) *Operational Level*: This level consists of two local controllers, namely automatic lane keeping (ALK) controller and combined automation-driver (CAD) controller. These are, respectively, dedicated to two different control goals: lane tracking and management of conflict issue. Especially, the CAD controller allows the driver to have full control authority when she/he desires to realize some specific driving maneuvers.

2) *Tactical Level*: This level aims to orchestrate the smooth control authority transition between two local controllers of the operational level to perform a given task. The tactical level is composed of two modules: DMS and decision-making algorithm (DMA).

Hereafter, the design of the supervisor of the tactical level is presented. The integration of this original supervisor into the control design procedure characterizes the *human-automation oriented design* feature of the proposed shared control method.

#### B. Supervisor Design for Shared Control Authority

The supervisor plays a *strategic role* in coordinating the ALK and the CAD controllers to perform a given driving task.

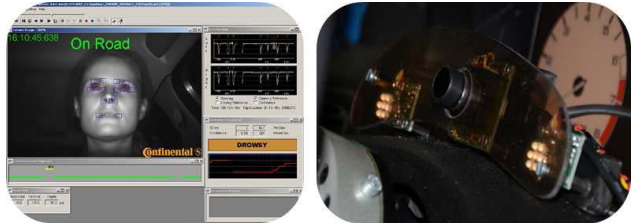


Fig. 7. DMS from Continental company.

This aims to provide a *weighting signal* which represents the information not only on the driver's state but also on the driving environment perception. Then, this signal will be used to unify two local controllers of the operational level.

1) *Decision-Making Algorithm*: This decision-making algorithm allows for a smooth transition between the ALK and the CAD controllers according to different driving circumstances. It is designed by exploiting the information from three units: DMS, risk evaluation, and conflict detection.

a) *Driver monitoring system*: This system has been the topic of intensive investigations in recent years [24], [25]. Here, we only highlight its main components that have been designed for the SHERPA driving simulator (see Fig. 7).

The DMS guarantees that the driver is not drowsy, and she/he is fully aware of the driving situation. It is also used to verify if the driver is currently watching the road, even though she/he is not actively involved in the driving task. In the case where the driver state from the DMS is not OK, an alarm process is systematically activated. The information from the DMS is crucial to the transition mechanism between two local controllers. Indeed, this allows the driver to regain the vehicle control when a mandatory authority transition from the automation to the driver is required. Specifically, two following DMS indicators are used for the supervisor design.

(i) *Driver drowsiness monitoring (DDM)*. This indicator indicates if there is a problem of driver's vigilance.

- $DDM = 0$  if the driver is *watchful*.
- $DDM = 1$  if the driver is *slightly drowsy*.
- $DDM = 2$  if the driver is *drowsy*.
- $DDM = 3$  if the driver is *sleepy*.

The reliability of this indicator is quantified by the driver drowsiness monitoring valid, i.e.,  $0 \leq DDM_v \leq 100\%$ . When  $DDM_v \geq 80\%$  (threshold determined empirically), the information given by the DDM is considered as *valid*, which means that  $DDM_v$  is OK. However, when  $DDM_v < 80\%$  (i.e.,  $DDM_v$  is not OK), this is not considered. The binary value of DDM, denoted by  $DDM_b$ , constituting a decision on the driver drowsiness state is defined as follows:

$$DDM_b = \begin{cases} 0, & \text{if } DDM < 2 \\ 1, & \text{if } DDM \geq 2 \end{cases} \quad (13)$$

(ii) *Driver inattention monitoring (DIM)*. This indicator indicates if the driver is inattentive (off road = 1) or not (on road = 0). The visual distraction level of drivers is nonlinear by its nature [38], as it increases

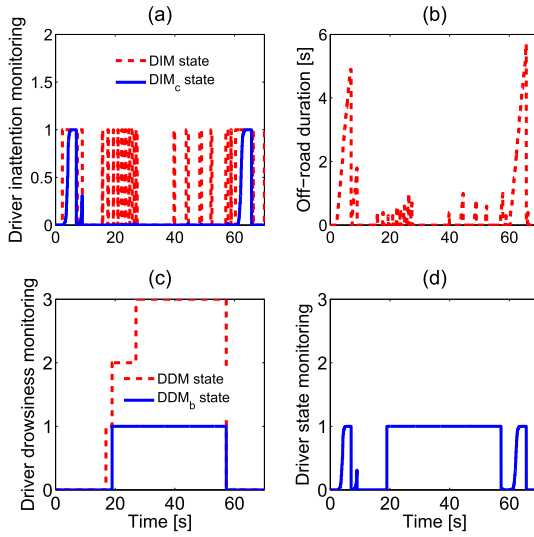


Fig. 8. Experimental validation on performance of driver monitoring obtained with Continental DMS.

exponentially with time when the driver looks away from the road scene, but decreases nearly instantaneously when she/he refocuses on the visual field of the road. For the studied Continental DMS, this behavior of driver distraction is modeled as follows:

$$\text{DIM}_c = \frac{1}{1 + e^{-a(b \cdot T \cdot \text{DIM} - c)}} \quad (14)$$

where  $T$  is the duration in which the DIM is activated ( $\text{DIM} = 1$ ), i.e., the driver is inattentive. Note that if  $T > 2$  s, then the driver is considered as distracted [2]. Hence, the values of  $a$ ,  $b$ , and  $c$  in (14) have been chosen to guarantee that the convergence rate of  $\text{DIM}_c$  is 3 s to avoid a *false alarm* on the detection of driver distraction.

Two outputs  $\text{DDM}_b$  and  $\text{DIM}_c$  of the DMS are used to manage the control authority transition between two local controllers via the driver state monitoring variable DSM

$$\text{DSM} = \text{DIM}_c + (1 - \text{DIM}_c) \left(1 - e^{-\frac{\text{DDM}_b}{\epsilon}}\right) \quad (15)$$

where  $\epsilon = 0.1$  is a tuning parameter. Remark from (15) that in the case of driver's hypovigilance (i.e.,  $\text{DDM}_b = 1$ ), the DSM becomes systematically 1. This means that a problem on the driver's state is detected. Moreover, if there is no problem of driver's hypovigilance (i.e.,  $\text{DDM}_b = 0$ ), only  $\text{DIM}_c$  is considered in the variable DSM.

The experimental results on the performance of driver monitoring obtained with Continental DMS are depicted in Fig. 8. This is confirmed by the results in Fig. 8(a) indicating the information on  $\text{DIM}_c$  computed from DIM and the driver's off-road duration  $T$  [see Fig. 8(b)]. Remark that  $\text{DIM}_c$  tends to 1 whenever  $T > 3$  s. The information on  $\text{DDM}_b$  defined in (13) is represented in Fig. 8(c). Finally, the corresponding result of DSM shown in Fig. 8(d) represents clearly its relationship with  $\text{DIM}_c$  and  $\text{DDM}_b$  given in (15).

*b) Risk evaluation:* This unit provides to the DMA an evaluation on the risk of lane departure. It takes into account the constraints related to the vehicle positioning and heading.

At each time sample, the vehicle front-wheel positions  $y_{ll}$  and  $y_{rr}$  and the relative yaw angle  $\psi_L$  are computed from the location of the CG using the kinematic formulas for the left and right lane boundaries [39]

$$\begin{aligned} y_{ll} &= y_{gl} - l_f \sin \psi_L - \frac{S_b}{2} \cos \psi_L \geq 0 \\ y_{rr} &= y_{gr} + l_f \sin \psi_L - \frac{S_b}{2} \cos \psi_L \geq 0 \end{aligned} \quad (16)$$

with

$$y_{gl} = L/2 - (y_L - l_p \psi_L), \quad y_{gr} = L/2 + (y_L - l_p \psi_L) \quad (17)$$

where  $L$  is the lane width and  $S_b$  is the length of vehicle axles. Since  $\psi_L$  is small, by substituting (17) into (16), it follows that:

$$-\frac{L - S_b}{2} \leq y_L + (l_f - l_p) \psi_L \leq \frac{L - S_b}{2}. \quad (18)$$

From (9) and (18), the limit of  $\theta_{\text{near}}$  can be easily obtained as  $|\theta_{\text{near}}| \leq \theta_{\text{lim}}$  where

$$\theta_{\text{lim}} = \frac{L - S_b}{2v_x T_p} + \left(1 - \frac{l_f}{v_x T_p}\right) |\psi_L \text{ lim}|.$$

The risk is evaluated by  $\theta_{\text{lim}}$  which is based on the heading error limit  $\psi_L \text{ lim}$ . Road accident data have shown that most of the run-off-road accidents start with  $\psi_L \text{ lim} = 5^\circ$  [39].

*c) Conflict detection:* The time indicator index representing the sharing quality in terms of conflict management between the driver and the LKA system can be defined by their torque product as follows:

$$\mathcal{I} = T_d T_a. \quad (19)$$

Note that a negative value of  $\mathcal{I}$  in (19) indicates that the LKA system is in a conflicting situation with the human driver.

*2) Smooth Control Authority Transition:* Based on the above-mentioned information on the driver state monitoring, the risk evaluation, and the conflict index, the indicator signal orchestrating the smooth transition between the ALK and the CAD controllers is designed as follows:

$$\sigma_d = \begin{cases} 0 & \text{if } (\text{DSM} = 1) \vee ((|\theta_{\text{near}}| \geq \theta_{\text{lim}}) \wedge (\mathcal{I} \geq \lambda)) \\ 1 & \text{if } (\text{DSM} = 0) \wedge ((|\theta_{\text{near}}| < \theta_{\text{lim}}) \\ & \vee ((|\theta_{\text{near}}| \geq \theta_{\text{lim}}) \wedge (\mathcal{I} < \lambda))) \end{cases} \quad (20)$$

where  $\lambda$  is the maximal level of negative interference between the driver and the LKA system. In this paper, based on the hand stiffness feeling of the driver, the value of  $\lambda = -2$  is experimentally identified. Remark from (20) that  $\sigma_d = 0$  (corresponding to the ALK controller) when the driver's distraction/drowsiness is detected by the DMS, or in the case where the risk from the driving environment is high. One has  $\sigma_d = 1$  (corresponding to the CAD controller) when the driver is watchful, not distracted and correctly steers the vehicle, or when a conflicting situation is detected. It is important to note that the ALK controller is systematically activated after 0.8 s (i.e. the average reaction time of drivers) from the moment where the haptic interface system does not detect the presence of at least one driver's hand on the steering wheel.

Note that the *hard* switching function (20) could result in undesirable chattering phenomena when the switching frequency between two local controllers is important. Hence, a low-pass filter is used to *smooth out* the transition signal  $\sigma_d$

$$\frac{\sigma(s)}{\sigma_d(s)} = \frac{1}{1 + \tau_\sigma s} \quad (21)$$

where  $\tau_\sigma = 0.8$  s is the driver's response time. The switching law [see (20) and (21)] allows for a smooth control authority transition between two local controllers to improve the driving comfort.

Assume that the ALK (respectively, CAD) controller provides an amount of assistance torque  $T_{a1}$  (respectively,  $T_{a2}$ ). Using the smooth transition law [see (20) and (21)], the unified control action of these two controllers is given by

$$u = T_a = \alpha_1 T_{a1} + \alpha_2 T_{a2} \quad (22)$$

where  $\alpha_1 = 1 - \sigma$  and  $\alpha_2 = \sigma$ , thus  $\alpha_1 + \alpha_2 = 1$ . Remark from (22) that the input  $T_a$  of (12) corresponds to a *convex combination* of  $T_{a1}$  and  $T_{a2}$ . Thus, the basic idea behind the proposed authority transition strategy can be interpreted as a weighting approach of steering assistance torques orchestrated by the smooth signal  $\sigma$  in (20) and (21).

#### IV. OPTIMAL-BASED CONTROL DESIGN

This section presents the design of both ALK and CAD controllers of the operational level. To this end, the performance output of the driver-vehicle system (12) is first defined. Then, an optimal-based control procedure is detailed.

##### A. Characterization of Closed-Loop Performance

The performance of the control law (22) strongly depends on the definition of the performance variable. An appropriate definition of this variable for each local controller (ALK or CAD) has a key role to achieve the control goals defined in Section III. To this end, let us consider the HiLV model (12) with its performance vector of the following form:

$$\begin{aligned} \dot{x} &= Ax + B_u u + B_w w \\ z_\alpha &= C_\alpha x + D_\alpha u + E_\alpha w \end{aligned} \quad (23)$$

where the *time-varying* performance matrices are defined as

$$\begin{aligned} z_\alpha &= \alpha_1 z_1 + \alpha_2 z_2, \quad C_\alpha = \alpha_1 C_1 + \alpha_2 C_2 \\ D_\alpha &= \alpha_1 D_1 + \alpha_2 D_2, \quad E_\alpha = \alpha_1 E_1 + \alpha_2 E_2. \end{aligned} \quad (24)$$

To be comply with the control expression (22), the performance matrices in (24) with index 1 (respectively, 2) corresponds to the ALK controller (respectively, the CAD controller). In the sequel, we show how to characterize the closed-loop performance via the definition of the performance matrices  $C_i$ ,  $D_i$ , and  $E_i$  with  $i = 1, 2$ .

To improve the interaction between human drivers and the LKA system, the performance variable should represent the lane tracking performance, the driving comfort, and the interference level indicating the quality of shared steering control. For that, this variable can be in the form

$$z_i = \mathcal{W}_i y, \quad i = 1, 2 \quad (25)$$

where

$$\begin{aligned} \mathcal{W}_i &= \text{diag}(W_{iay}, W_{i\dot{\psi}_L}, W_{i\theta_{\text{near}}}, W_{i\theta_{\text{far}}}, W_{i\dot{\delta}_d}, W_{i\Delta T}) \\ y &= [a_y \ \dot{\psi}_L \ \theta_{\text{near}} \ \theta_{\text{far}} \ \dot{\delta}_d \ T_d - \lambda_c T_a]^\top. \end{aligned}$$

The weighting matrices  $\mathcal{W}_1$  and  $\mathcal{W}_2$  are tuned according to the control objectives of each local controller. The form of the performance variable  $z_i$  in (25) deserves particular attention.

- 1) The tracking performance is represented by  $\theta_{\text{near}}$  in (9) (weighted by  $W_{i\theta_{\text{near}}}$ ) whereas  $\theta_{\text{far}}$  in (10) (weighted by  $W_{i\theta_{\text{far}}}$ ) provides the driver's anticipatory behavior.
- 2) The driving comfort is represented by the lateral acceleration  $a_y$  (weighted by  $W_{iay}$ ) and the relative yaw rate  $\dot{\psi}_L$  to the target line (weighted by  $W_{i\dot{\psi}_L}$ ). The introduction of  $\dot{\delta}_d$  (weighted by  $W_{i\dot{\delta}_d}$ ) guarantees a desired steering comfort and improves the vehicle damping response.
- 3) The conflict between the LKA system and the human driver can be characterized by  $(T_d - \lambda_c T_a)$  which is weighted by  $W_{i\Delta T}$ . As will be seen later, this torque quantity allows for a quadratic performance index including the following term:

$$W_{i\Delta T}^2 (T_d - \lambda_c T_a)^2 = W_{i\Delta T}^2 (T_d^2 + \lambda_c^2 T_a^2 - 2\lambda_c T_d T_a). \quad (26)$$

For some scalar  $\lambda_c > 0$ , a necessary condition to minimize the cost in (26) is to guarantee the positivity of the torque product  $T_d T_a$ . This allows to avoid the conflicting situation between the driver and the LKA system (see Section III-B). Moreover, the conflict level between two driving actors can be evaluated by the driver's feeling of resistance torque coming from the assistance. Remark from (26) that the introduction of  $\lambda_c$  offers a degree of freedom to penalize the generation of opposite assistance torque. Therefore, the effects of negative interference can be minimized. Furthermore, this also provides more control authority to the driver to perform some specific driving maneuvers in case of necessity.

Note that all components of  $y$  in (25) can be easily expressed by those of the state vector  $x$  in (12). Therefore, the performance matrices in (24) can be deduced as follows:

$$C_i = \mathcal{W}_i C_{yx}, \quad D_i = \mathcal{W}_i D_{yu}, \quad E_i = \mathcal{W}_i E_{yw}, \quad i = 1, 2$$

where

$$C_{yx} = \begin{bmatrix} 0 & v_x & 0 & 0 & 0 & 0 & 0 & 0 \\ 0 & 1 & 0 & 0 & 0 & 0 & 0 & 0 \\ 0 & 0 & \frac{v_x T_p - l_p}{v_x T_p} & \frac{1}{v_x T_p} & 0 & 0 & 0 & 0 \\ \theta_1 & \theta_2 & 0 & 0 & \theta_3 & 0 & 0 & 0 \\ 0 & 0 & 0 & 0 & 0 & 1 & 0 & 0 \\ 0 & 0 & 0 & 0 & 0 & 0 & 0 & 1 \end{bmatrix}$$

$$D_{yu} = [0 \ 0 \ 0 \ 0 \ 0 \ -\lambda_c]^\top$$

$$E_{yw} = [0 \ -v_x \ 0 \ 0 \ 0 \ 0]^\top.$$

Now, the form of all performance matrices is defined, the remaining task consists in parameterizing  $\mathcal{W}_1$  and  $\mathcal{W}_2$  to achieve the predefined control goals for each local controller.

1) *Automatic Lane Keeping Controller*: This controller aims to ensure the lane tracking performance. For that, the controller assists the driver or fully takes care of the lane keeping task. To achieve this objective, the matrix  $\mathcal{W}_1$  is parameterized to provide the best control performance in terms of lane tracking. Especially,  $W_{1\Delta T} = 0$  in this case, thus the authority sharing index (26) is not considered.

2) *Combined Automation-Driver Controller*: This allows a shared control between the driver and the LKA system, and a full control resumption of the driver. Note that in many situations, the driver may suddenly change the steering action, e.g., perform a lane change maneuver to avoid an undetected obstacle. These abrupt changes could generate serious conflicts between two driving actors. These changes could also saturate steering rate constraints which are limited by the available steering actuators. In such a scenario, only low level of assistance torque is required so that the driver remains the *master of the situation*. Therefore, the weighting matrix  $\mathcal{W}_2$  is parameterized (by tuning the parameters  $W_{2\Delta T}$  and  $\lambda_c$ ) to promote the driver's action with respect to that of the LKA system. Then, the driver can have more control authority to realize his/her intention and the LKA system assists him/her to achieve the steering maneuver without causing conflicts.

### B. Optimal-Based Control Design

Hereafter, the design of two local controllers is presented. To do that, we consider the following performance index:

$$\mathcal{J}_\alpha = \int_0^\infty z_\alpha(\tau)^\top z_\alpha(\tau) d\tau = \int_0^\infty \xi(\tau)^\top \mathbb{Q} \xi(\tau) d\tau \quad (27)$$

with

$$\xi = \begin{bmatrix} x \\ u \\ w \end{bmatrix}, \quad \mathbb{Q} = \begin{bmatrix} Q_\alpha & S_\alpha & N_\alpha \\ S_\alpha^\top & R_\alpha & M_\alpha \\ N_\alpha^\top & M_\alpha^\top & G_\alpha \end{bmatrix}.$$

The weighting matrices of the performance index are given by

$$\begin{aligned} Q_\alpha &= C_\alpha^\top C_\alpha, & S_\alpha &= C_\alpha^\top D_\alpha, & N_\alpha &= C_\alpha^\top E_\alpha \\ R_\alpha &= D_\alpha^\top D_\alpha, & M_\alpha &= D_\alpha^\top E_\alpha, & G_\alpha &= E_\alpha^\top E_\alpha. \end{aligned}$$

*Remark 3*: With the expression of  $z_\alpha$  in (24), the performance index  $\mathcal{J}_\alpha$  defined in (27) allows considering all possible couplings between the variables  $x$ ,  $u$ , and  $w$ . Especially, the coupling between the driver and the assistance torques, which represents the conflict issue, can be directly managed by the weighting matrix  $S_\alpha$ .

Let us rewrite (22) in the following state-feedback form:

$$u = (\alpha_1 K_1 + \alpha_2 K_2) x = K_\alpha x \quad (28)$$

where  $T_{a1} = K_1 x$ ,  $T_{a2} = K_2 x$ , and the parameter-dependent feedback gain  $K_\alpha$  will be designed such that the closed-loop system (23) satisfies the performance specifications defined in Section III-A. To this end, we design a controller of the form (28) which minimizes the performance index  $\mathcal{J}_\alpha$ . Note that this corresponds to the standard  $\mathcal{H}_\infty$  control problem. Assume that there exists the Lyapunov function of the following form:

$$\mathbb{V}(x) = x^\top P x, \quad P > 0$$

satisfying the Hamilton-Jacobi's inequality

$$\dot{\mathbb{V}}(x) + z_\alpha^\top z_\alpha < \gamma w^\top w - 2\zeta \mathbb{V}(x) \quad (29)$$

where  $\gamma$  and  $\zeta$  are positive scalars. Since  $\mathbb{V}(x) \geq 0$ , integrating both the sides of (29) from 0 to  $\infty$ , it follows that:

$$\int_0^\infty z_\alpha(\tau)^\top z_\alpha(\tau) d\tau < \mathbb{V}(0) - \mathbb{V}(\infty) + \gamma \int_0^\infty w(\tau)^\top w(\tau) d\tau.$$

Then, the upper bound of the performance index is given by

$$\mathcal{J}_\alpha < x_0^\top P x_0 + \gamma \eta \quad (30)$$

where  $x_0$  is the initial condition of (23), and the positive scalar  $\eta$  represents the energy upper bound of the disturbance  $w$ . Remark from (30) that for some given  $x_0$  and  $\eta$ , we can minimize  $\mathcal{J}_\alpha$  by minimizing the scalar  $\gamma$ .

Using the control expression (28) and substituting the closed-loop matrices (23) into (29), it follows that:

$$\begin{aligned} \Xi &= \dot{x}^\top P x + x^\top P \dot{x} + z_\alpha^\top z_\alpha - \gamma w^\top w + 2\zeta \mathbb{V}(x) \\ &= \text{He}([(A + B_u K_\alpha)x + B_w w]^\top P x + \zeta x^\top P x) \\ &\quad + [(C_\alpha + D_\alpha K_\alpha)x + E_\alpha w]^\top (*) - \gamma w^\top w < 0 \end{aligned} \quad (31)$$

Inequality (31) can be rewritten in the compact form

$$\Xi = \begin{bmatrix} x \\ w \end{bmatrix}^\top \Theta \begin{bmatrix} x \\ w \end{bmatrix} < 0. \quad (32)$$

Then, it is clear from (32) that (29) is verified if

$$\begin{aligned} \Theta &= \begin{bmatrix} \text{He}(PA + PB_u K_\alpha + \zeta P) & PB_w \\ B_w^\top P & -\gamma I \end{bmatrix} \\ &\quad + \begin{bmatrix} C_\alpha^\top + K_\alpha^\top D_\alpha^\top \\ E_\alpha^\top \end{bmatrix} [C_\alpha + D_\alpha K_\alpha \quad E_\alpha] < 0. \end{aligned} \quad (33)$$

By Schur complement lemma [26], condition (33) can be proved to be equivalent to

$$\begin{bmatrix} \text{He}(PA + PB_u K_\alpha + \zeta P) & * & * \\ B_w^\top P & -\gamma I & * \\ C_\alpha + D_\alpha K_\alpha & E_\alpha & -I \end{bmatrix} < 0. \quad (34)$$

Let us define  $X = P^{-1}$ . Pre- and postmultiplying (34) with  $\text{diag}(X, I, I)$ , followed by the variable change:

$$M_\alpha = K_\alpha X \quad (35)$$

we can prove that (34) is equivalent to

$$\begin{bmatrix} \text{He}(AX + B_u M_\alpha + \zeta X) & * & * \\ B_w^\top & -\gamma I & * \\ C_\alpha X + D_\alpha M_\alpha & E_\alpha & -I \end{bmatrix} < 0. \quad (36)$$

Note that inequality (36) is represented in the form of *parameterized LMI* [40]:

$$\sum_{i=1}^2 \sum_{j=1}^2 \alpha_i \alpha_j \Psi_{ij} \quad (37)$$

where the quantity  $\Psi_{ij}$  is given by

$$\Psi_{ij} = \begin{bmatrix} \text{He}(AX + B_u M_j + \zeta X) & * & * \\ B_w^\top & -\gamma I & * \\ C_i X + D_i M_j & E_i & -I \end{bmatrix}. \quad (38)$$

By the relaxation result in [40], it follows that condition (37) is verified if:

$$\begin{aligned} \Psi_{ii} &< 0, \quad i \in \{1, 2\} \\ 2\Psi_{ii} + \Psi_{ij} + \Psi_{ji} &< 0, \quad i, j \in \{1, 2\} \text{ and } i \neq j. \end{aligned} \quad (39)$$

The results of the above-mentioned theoretical developments can be summarized in Theorem 1.

**Theorem 1:** Given system (23) and a positive scalar  $\zeta$ . The control law (28) is stabilizing with respect to (23) while minimizing the performance index (27) if there exist positive definite matrix  $X$ , matrices  $M_1$  and  $M_2$ , and a positive scalar  $\gamma$  satisfying the following convex optimization:

$$\min_{X, M_1, M_2} \gamma \quad (40)$$

subject to the LMIs (39) with  $\Psi_{ij}$  given in (38). Moreover, the feedback gains can be computed from (35) as

$$K_i = M_i X^{-1}, \quad i = 1, 2.$$

**Remark 4:** The design conditions presented in Theorem 1 are completely *independent* of the smooth transition signal  $\sigma$  defined in (21). This interesting fact means that the control actions can be computed by switching arbitrarily between the two controllers, without fear of causing closed-loop instability.

**Remark 5:** Theorem 1 provides a systematic method to design two feedback gains for the ALK and the CAD controllers, respectively. The design procedure is formulated as a convex optimization problem (40) in the function of decision variables  $P$ ,  $M_1$ ,  $M_2$ , and  $\gamma$ . Therefore, the feedback gains  $K_1$  and  $K_2$  can be effectively computed with available numerical toolboxes, for example YALMIP toolbox [41].

**Remark 6:** The parameter  $\zeta$ , called *decay rate*, is related to the time performance of system (23). A large value of this tuning parameter leads to a fast closed-loop convergence speed; however, the corresponding controller could induce some aggressive behaviors. Especially, this situation can get worst if the disturbance is involved in the vehicle dynamics.

## V. HARDWARE EXPERIMENTS AND DISCUSSION

To demonstrate the effectiveness of the proposed control approach, the two-level cooperative control scheme described in Section III is implemented on the SHERPA interactive dynamic driving simulator and tested with human drivers. The SHERPA simulator is in the form of a Peugeot 206 vehicle fixed on a Stewart platform, the overall is positioned in front of five flat panel displays providing a visual field of 240° [see Fig. 9 (left)]. This simulator is equipped with a sensor providing the measurements of the steering angle, the steering rate, and the steering torque [see Fig. 9 (right)]. Its force-feedback steering wheel can reproduce the self-aligning torque  $T_s$  provided by a nonlinear vehicle dynamic model and, at the same time, allows the human driver to apply an additional torque for the steering process. The available Continental DMS is connected to a CAN bus and provides the measurements on the driver drowsiness and distraction.



Fig. 9. Left: SHERPA driving simulator. Right: steering torque sensor.

### A. Robustness Performance Analysis

1) *Robustness with respect to Driver Parametric Uncertainty:* Since the variation of driver parameters has not been explicitly considered for the control design in Section III, it is therefore worth checking *a posteriori* the closed-loop stability of the driver-vehicle system in the presence of such parametric uncertainties. To do that, the well-known  $\mu$ -analysis method [42] is used to evaluate the stability margin. Note that similar stability analysis has been reported in [8].

$\Sigma$  denotes the nominal linear closed-loop system and  $\Delta$  denotes the uncertainty structure. The structural singularity value at the frequency  $\omega$  is defined as follows:

$$\mu_\Delta(\Sigma(j\omega)) = \left( \min \left( \frac{\max \bar{\sigma}[\Delta(j\omega)]}{\det(I - \Delta\Sigma(j\omega))} = 0 \right) \right)^{-1}$$

where  $\max \bar{\sigma}[\Delta(j\omega)]$  is the maximum singularity of  $\Delta(j\omega)$ . The stability margin with respect to  $\Delta$  affecting on  $\Sigma$  is guaranteed if

$$\mu_\Delta(\Sigma(j\omega)) < 1, \quad \forall \omega.$$

Since computing the exact value of  $\mu_\Delta$  is known as an NP complex problem, its upper bound  $\mu_{\Delta \max}$  and lower bound  $\mu_{\Delta \min}$  are usually used to evaluate the robustness performance [42]. Indeed,  $1/\mu_{\Delta \max}$  (respectively,  $1/\mu_{\Delta \min}$ ) allows for a pessimistic (respectively, optimistic) evaluation of the robustness margin. For the computation of  $\mu_{\Delta \max}$  and  $\mu_{\Delta \min}$ , the driver parameters  $T_l$ ,  $T_i$ ,  $T_n$ ,  $K_a$ ,  $K_c$ ,  $\tau_a$ , and  $T_p$  in (6) and (11) are assumed constant but uncertain of the form

$$\begin{aligned} T_l &= \bar{T}_l (1 + \vartheta_{T_l} \delta_{T_l}), \quad T_i = \bar{T}_i (1 + \vartheta_{T_i} \delta_{T_i}) \\ T_n &= \bar{T}_n (1 + \vartheta_{T_n} \delta_{T_n}), \quad T_p = \bar{T}_p (1 + \vartheta_{T_p} \delta_{T_p}) \\ K_a &= \bar{K}_a (1 + \vartheta_{K_a} \delta_{K_a}), \quad K_c = \bar{K}_c (1 + \vartheta_{K_c} \delta_{K_c}) \\ \tau_a &= \bar{\tau}_a (1 + \vartheta_{\tau_a} \delta_{\tau_a}) \end{aligned}$$

where  $-1 \leq \delta_i \leq 1$ , for  $i \in \{T_l, T_i, T_n, T_p, K_a, K_c, \tau_a\}$ , represent the model parametric uncertainties;  $\bar{T}_l$ ,  $\bar{T}_i$ ,  $\bar{T}_n$ ,  $\bar{T}_p$ ,  $\bar{K}_a$ ,  $\bar{K}_c$ , and  $\bar{\tau}_a$  are nominal values; and  $\vartheta_{T_l}$ ,  $\vartheta_{T_i}$ ,  $\vartheta_{T_n}$ ,  $\vartheta_{T_p}$ ,  $\vartheta_{K_a}$ ,  $\vartheta_{K_c}$ , and  $\vartheta_{\tau_a}$  represent the possible variations around nominal values. Here, the following parameter variations are considered:

$$\begin{aligned} \vartheta_{T_l} &= 30\%, \quad \vartheta_{T_i} = 30\%, \quad \vartheta_{T_n} = 10\%, \quad \vartheta_{T_p} = 30\% \\ \vartheta_{K_c} &= 30\%, \quad \vartheta_{K_a} = 30\%, \quad \vartheta_{\tau_a} = 20\%. \end{aligned}$$

Note that the above-mentioned parameter variations represent a wide panel of driver population. Now, we compute  $\mu_{\Delta \max}$  and  $\mu_{\Delta \min}$  over the frequency interval  $\omega \in [10^{-2}, 10^2]$  (which covers largely the operating ranges of both vehicle system

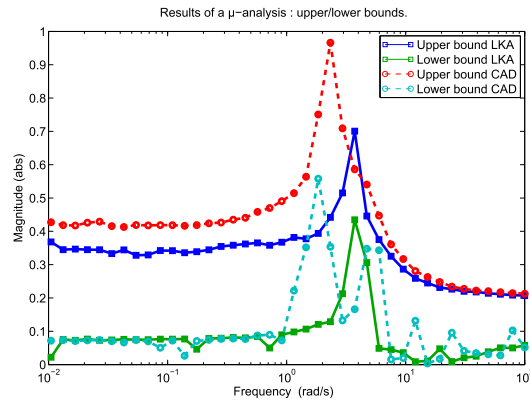


Fig. 10.  $\mu$ -analysis for robustness performance with respect to the parametric uncertainty of the driver model.

TABLE III  
SENSITIVITY with respect to DRIVER UNCERTAIN PARAMETERS

Parameter	Nominal value	Stability range	$S_{ALK}$	$S_{CAD}$
$T_l$	1.57	[0.92 – 2.62]	5%	22%
$T_i$	0.18	[0.06 – 0.53]	4%	5%
$K_a$	15.70	[6.36 – 28.62]	9%	13%
$K_c$	6.83	[1.725 – 13.9]	5%	8%
$T_n$	0.11	[0.035 – 0.13]	10%	11%
$T_p$	0.78	[0.37 – 1.14]	8%	18%
$\tau_a$	1.05	[0.28 – 2.22]	1%	4%

and human drivers) for two cases: 1) a closed-loop system obtained with the LKA controller, and 2) a closed-loop system obtained with the CAD controller. The corresponding results on  $\mu$ -analysis are depicted in Fig. 10. From pessimistic viewpoint, we observe that  $\mu_{\Delta \max} < 1$  for both the cases over the considered frequency interval. The worst situation with respect to the ALK (respectively, CAD) controller corresponds to the peak value of 0.69 (respectively, 0.96) occurring in the vicinity of the frequency at  $\omega = 4$  [rad/s] (respectively,  $\omega = 2.5$  [rad/s]). This means that robust stability with respect to the above-mentioned driver parametric uncertainties is guaranteed for designed controllers. From the optimistic robustness evaluation (see lower bounds  $\mu_{\Delta \min}$  in Fig. 10), for both the cases, the robustness margins can be doubled while still guaranteeing the closed-loop stability. This means that from an optimistic viewpoint, the designed controllers could be used for almost all driver populations.

The sensitivity study of the driver parameters is performed using MATLAB  $\mu$ -analysis toolbox. The corresponding results given in Table III show a low sensitivity of the closed-loop system with respect to the driver parameters. Indeed, the sensibility  $S_{ALK}$  (respectively,  $S_{CAD}$ ) of the parameters in the case of ALK (respectively, CAD) controller does not exceed 10% (respectively, 22%). For example,  $S_{CAD,T_l} = 22\%$  means that if the variation interval of  $T_l$  is increased to 100%, then the system robustness is reduced 22% of its stability margin. Note also that the CAD controller is more sensible to the driver parameters than the ALK one, since it is designed to work jointly with driver without generating negative interferences. Moreover, the sensibility analysis of each driver parameter allows to determine its variation interval

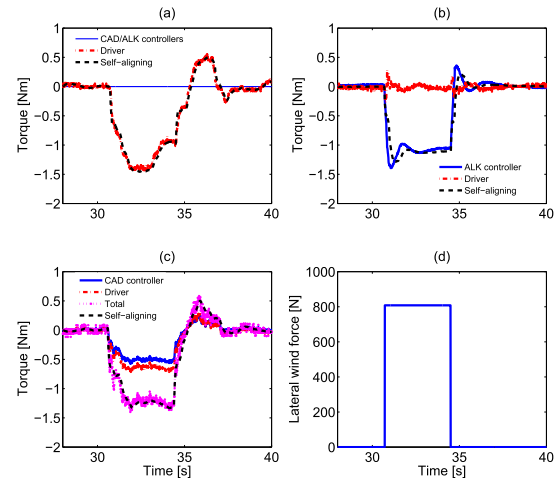


Fig. 11. Experimental results on disturbance rejection. (a) Steering torques in manual control test (without assistance). (b) Steering torques in full automatic control test with the ALK controller. (c) Steering torques in shared control test with the CAD controller. (d) Wind force disturbance.

for which the closed-loop stability is guaranteed with designed controllers (see Table III). It is clear that these parameter intervals cover a wide range of driving styles.

2) *Robustness with respect to Important Wind Force Disturbance:* For this test, the vehicle is on a straight road section at a constant speed  $v_x = 15$  [m/s]. Assume also that the vehicle is subjected to a strong lateral wind force  $f_w = 800$  [N], occurring from  $t = 30.5$  s to  $t = 34.5$  s [see Fig. 11(d)]. This wind force generates a yaw moment disturbance directly impacting the self-aligning torque  $T_s$ . The latter is a resistance torque which can be felt by the driver through the steering column system.

Now, the robustness of each controller of the operational part, i.e., the human driver, the ALK controller, and the CAD controller, is separately examined via three following cases.

- *Case 1 (Driver-Automation Shared Control):* The CAD controller is used to assist the driver for controlling the vehicle. As clearly shown in Fig. 11(c), the driver only provides a part of the required torque amount (about 50% of  $T_s$ ) for the driving task. Especially, the CAD controller and the driver *cooperatively* work to counteract the lateral wind force disturbance, i.e., no conflict situation has been detected.
- *Case 2 (ALK Controller):* The vehicle is *fully* controlled by the ALK controller without human intervention [see Fig. 11(b)].
- *Case 3 (Manual Control):* The vehicle is *manually* controlled by a human driver. As indicated in Fig. 11(a), the driver must provide the same amount of torque as the self-aligning one to reject the wind disturbance effect. There are no control actions from both designed ALK and CAD controllers.

Fig. 12 shows the comparison of the vehicle responses obtained with three above-mentioned cases. Observe that the undesirable effect of the wind disturbance is rejected for all the three cases, since the corresponding lateral deviation error and heading error remain small during the whole test [see Fig. 12(a) and (b)]. Especially, in Case 2, the ALK

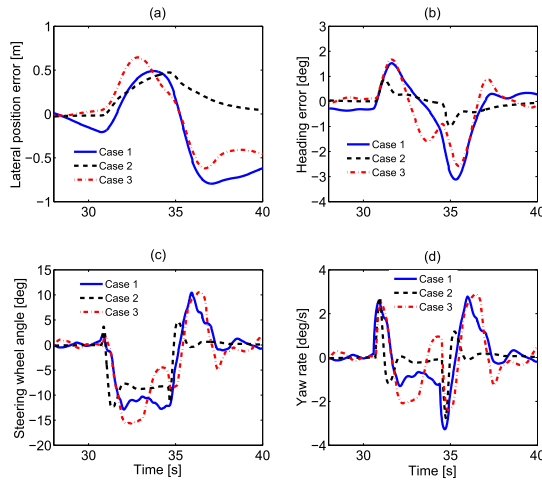


Fig. 12. Experimental results on disturbance rejection. Case 1: shared control between human driver and CAD controller (solid line). Case 2: only ALK controller (dashed line). Case 3: manual control (dashed dotted line).

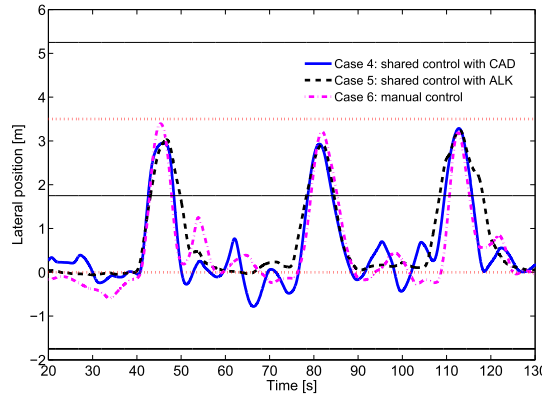


Fig. 13. Triple-lane change maneuver with three different control cases.

controller offers the best control performance with smallest tracking errors. Fig. 12(c) shows that the ALK controller provides a faster closed-loop responses compared with two other cases. Note also that for the considered driving situation, the closed-loop behaviors in Cases 1 and 3 are quite similar. This test scenario confirms clearly the role of each designed controller, namely the ALK controller is specifically used for lane tracking and the CAD controller is used for shared control purposes to assist human drivers.

### B. Experimental Evaluation for Shared Control Quality

This test demonstrates the performance of the CAD controller in terms of conflict management. To this end, the driver performs a triple lane change at  $v_x = 20$  [m/s] to avoid successively three obstacles that would not have been detected by the vision system (see Fig. 13). The following steering workload is used to evaluate the driver's steering feeling:

$$\mathcal{W}_s = \int_0^{\Delta T} T_d(\tau) T_a(\tau) \dot{\delta}_d(\tau) d\tau. \quad (41)$$

From the viewpoint of energy consumption, the indicator  $\mathcal{W}_s$  can be interpreted as the steering energy provided by the driver

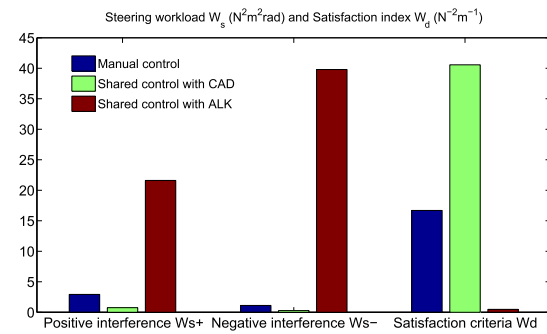


Fig. 14. Comparison of  $\mathcal{W}_s$  and  $\mathcal{W}_d$  between different control strategies corresponding to the experimental results presented in Fig. 13.

within a duration  $\Delta_T$  to perform a desirable steering maneuver. For the case of manual control, only the driver torque  $T_d$  and the steering rate  $\dot{\delta}_d$  are used to compute  $\mathcal{W}_s$ . The product  $T_d \dot{\delta}_d$  involved in (41) aims to take into account the conflict situations between the human driver and the LKA system in the computation of  $\mathcal{W}_s$ . If the driver voluntarily steers the wheel, she/he effectively performs some positive steering work  $\mathcal{W}_s^+$ . However, if the driver operates the steering wheel against unnatural fluctuations of the vehicle or the resistance of the LKA system in the case of conflict, unnecessary negative steering work  $\mathcal{W}_s^-$  will be performed. Hence, the positive and negative interference levels ( $\mathcal{W}_s^+$  and  $\mathcal{W}_s^-$ ) can be used to assess driver's steering feel [43]. Let us also define the following satisfaction criterion  $\mathcal{W}_d$  as the ratio of the lateral displacement to avoid the obstacles over the driver's effort:

$$\mathcal{W}_d = \frac{\int_0^{\Delta T} y_L(\tau) d\tau}{\int_0^{\Delta T} T_d(\tau)^2 d\tau}.$$

Fig. 14 depicts the comparison of the steering workload  $\mathcal{W}_s$  and the satisfaction criterion  $\mathcal{W}_d$  corresponding to the triple lane change maneuver of the three following cases.

- Case 4: Shared control between driver and CAD controller.
- Case 5: Shared control between driver and ALK controller.
- Case 6: Manual steering control.

Observe that the amounts of both  $\mathcal{W}_s^+$  and  $\mathcal{W}_s^-$  in Case 5 are much larger than those in Case 6. This means that a huge conflict between the driver and the LKA system has occurred in Case 5. In other words, the steerability of the vehicle becomes difficult in this case, since the ALK controller does not aim for shared control purposes. However, the workload amounts in Case 4 are significantly reduced compared with those in Case 6. This means that the CAD controller allows for a good level of comfort for shared lateral control with a better driver's steering feeling. Fig. 14 also shows that the satisfaction index  $\mathcal{W}_d$  obtained in Case 4 is greatly improved compared with that in Case 6, which is on the contrary to Case 5.

### C. Validation of the Two-Level Cooperative Control Strategy

To point out the validity of the designed control supervisor and both optimal-based ALK and CAD controllers, we distinguish the two following cases with complex driving scenarios.

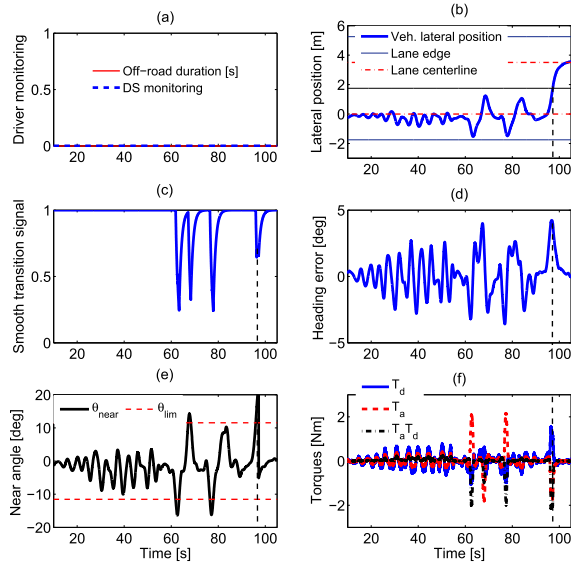


Fig. 15. Experimental validation of the two-level cooperative steering control strategy. Driver state is OK.

*1) Experimental Driving Scenario With  $DSM = 0$ :* For this experiment, the vehicle is on a straight road section at a fixed speed  $v_x = 15$  [m/s] and the driver is first asked to watch attentively the road, i.e., the driver monitoring diagnosis remains OK as indicated in Fig. 15(a). He initially performs a zigzag driving pattern without exceeding the angle limit  $\theta_{\text{lim}}$  (between  $t = 10$  s and  $t = 60$  s) and then beyond this limit (between  $t = 60$  s and  $t = 105$  s) [see Fig. 15(e)]. Observe from Fig. 15(f) that the driver and assistance torques always have the same sign during the first driving period from  $t = 10$  s to  $t = 60$  s. This means that the CAD controller assists the driver to achieve his desired steering maneuver when  $\theta_{\text{near}} \leq \theta_{\text{lim}}$ , i.e., there is no lane departure risk. However, in the case of risk (from  $t = 60$  s to  $t = 105$  s), the ALK controller is activated by the proposed shared control strategy [see Fig. 15(c)] to provide a haptic information (i.e., opposite torque) to the driver as shown in Fig. 15(f).

At  $t = 97$  s, the driver desires to perform a lane change maneuver [see Fig. 15(b)]. During this maneuver, the driver and assistance torques are in opposite sign [Fig. 15(f)] until the conflict has been detected by the control supervisor, i.e., the conflict indicator  $\mathcal{I} = T_d T_a$  reaches its predefined threshold  $\lambda = -2$ . Then, the CAD controller is reactivated (i.e.,  $\sigma$  tends again to 1) to allow the driver realizing easily his desired maneuver. Remark that  $\mathcal{I} > \lambda$  whenever the driver is fully aware of his driving task ( $DSM = 0$ ) [see Fig. 15(f)].

*2) Experimental Driving Scenario With  $DSM \neq 0$ :* This scenario also requires the driver to perform a zigzag driving pattern. However, he must purposely look at the side of the road (from  $t = 105$  s to  $t = 122$  s and from  $t = 135$  s to  $t = 151$  s) to simulate a driver's distraction [see Fig. 16(a)]. As indicated in Fig. 16(b), the control transition signal  $\sigma$  tends exponentially to 0 with a converging time  $\tau_\sigma = 0.8$  s whenever the off-road duration  $T > 3$  s. Thus, the driver state variable  $DSM$  tends to 1 and the vehicle control authority is fully given to the LKA system. In such a situation, the driver-automation

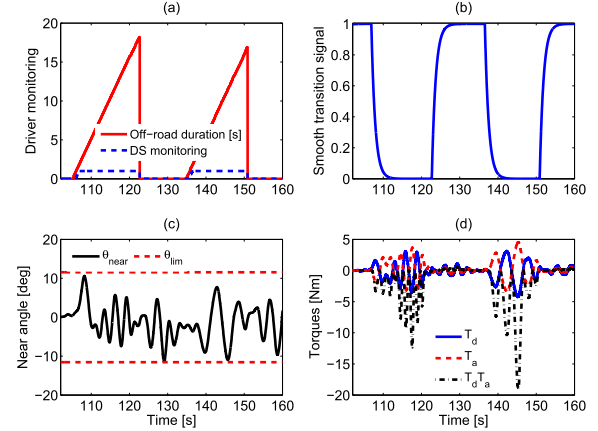


Fig. 16. Experimental validation of the two-level cooperative steering control strategy: Driver state is not OK.

conflict is detected, since the signs of their corresponding torques  $T_d$  and  $T_a$  are always opposite [see Fig. 16(d)]. Note also from Fig. 16(c) that  $\theta_{\text{near}} \leq \theta_{\text{lim}}$  for the whole test. This means that the proposed shared steering controller can prevent run-off-road accidents.

Remark that during the period of driver's distraction, the value of  $\mathcal{I}$  can largely exceed the threshold defined by the maximum allowable level of negative interference. Moreover, in this case, the ALK controller will be activated to effectively assist the distracted driver to maintain the vehicle on the lane. This confirms the design objectives of the smooth control authority transition signal defined in (20) and (21).

#### D. Driver-Automation Shared Control in Real-World Driving Conditions

This driving scenario aims to show the effectiveness of the proposed shared control method regarding its capacity to manage the control authority between the human driver and the automation system in real-world driving situations. The test has been done with a driver driving the SHERPA simulator on the Satory test track [see Fig. 17(a)]. Fig. 17(b) shows the corresponding vehicle speed which is variable and managed by the driver during the whole test. The driving scenario can be decomposed in three phases according to the driver's behaviors during the test.

- 1) *Phase 1:* Shared driving control with an attentive driver.
- 2) *Phase 2:* Driving with a distracted driver.
- 3) *Phase 3:* Automatic driving in absence of driver's hands on the steering wheel and driver's control resumption.

During Phase 1 ( $t < 50$  s which corresponds to the first four curves C1, C2, C3, and C4 shown in Fig. 4), the driver and the LKA system jointly perform the lane keeping task. Observe in Fig. 17(c) that the driver shares the vehicle control with the CAD controller while taking the bends C1, C2, and C4. For the third bend C3, the driver (intentionally) provides an insufficient steering torque for the driving task, thus the ALK controller is activated to avoid the lane departure as indicated in Fig. 17(d). Indeed, we can see in Fig. 18(a) that the authority transition signal  $\sigma$  tends to 0 when  $\theta_{\text{near}} > \theta_{\text{lim}}$  (i.e., the risk of lane departure is detected).

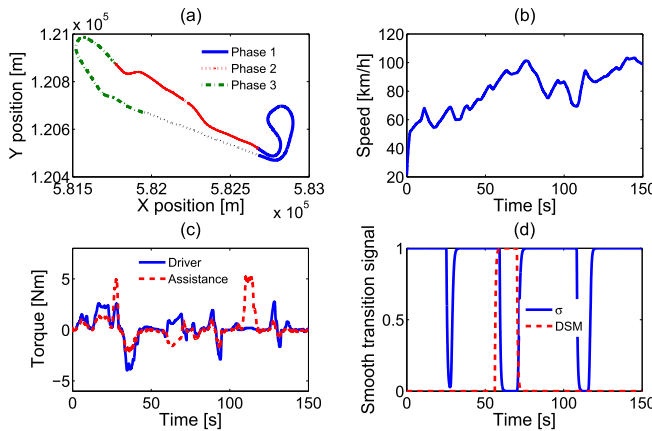


Fig. 17. Experimental results obtained with real-world Satory test track.

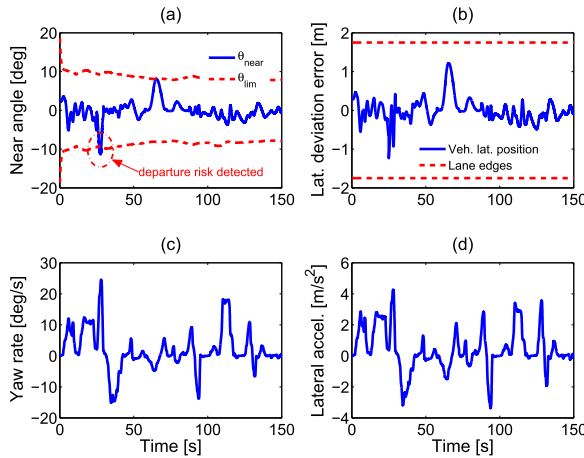


Fig. 18. Vehicle response with respect to the results shown in Fig. 17.

Phase 2 corresponds to the lane keeping on the road section covering the curves from C5 to C9. From  $t = 55$  s to  $t = 75$  s, the driver simulates a driver's distraction while taking curve C6 by turning his head outside the driving visual field while applying some torque to the steering wheel. In this situation, the variable DSM indicates a problem of driver's vigilance [see Fig. 17(d)]. Hence, the control authority of the LKA system is given to the ALK controller which provides an appropriate steering torque in the opposite sign of the driver's one to prevent the lane departure. After the period of driver's distraction, the DSM tends to 0, and the driver jointly controls the vehicle with the CAD controller.

During Phase 3, the driver releases both hands from the steering wheel just before taking curve C11 (from  $t = 105$  s to  $t = 120$  s); in this period, the LKA system solely controls the vehicle via the ALK controller [see Fig. 17(c)]. After the *autonomous* curve taking, the driver resumes the driving task, and the LKA system smoothly gives him the control authority, since  $\sigma$  tends again to 1 [see Fig. 17(d)]. Note that a good control performance in terms of lane keeping and lateral acceleration is obtained during Phase 3 as indicated in Fig. 18.

#### E. User Test Experiment

We present here some preliminary results of driver's acceptability obtained with the proposed shared control method



Fig. 19. Left: variable road sign inviting the driver to write the text message. Right: driver performing the ST.

via a user test. The goal is to assess potential benefits of the studied LKA system and how drivers would perceive the shared control method. To this end, the lane keeping performance is compared between manual driving as a baseline and driving with the developed LKA system under two driver attention conditions as detailed later.

This user test has been conducted with seven drivers (5 males and 2 females with an average age of 33 years and an average annual mileage of 13 500 [km]) on a traffic-free 4.5 [km] two lanes one way track with various curves [see Fig. 19 (left)]. The drivers must drive on the right lane with a fixed speed of 70 [km/h] to easily compare the steering behavior among the participants by avoiding interindividual differences in the choice of speed [13]. The study has been unfolded in two runs. For the first run, the participants must drive without any assistance (manual driving), whereas the studied LKA system has been activated to assist the drivers for the second run (shared control). Each run has been divided in two phases: the drivers are attentive during the first phase and they are distracted in the second one. In this paper, the driver's distraction has been induced by a secondary task (ST) which consists in reading and writing a short text message on a 10-in tablet while driving [see Fig. 19 (right)]. For each phase, the lane keeping performance is evaluated, and the drivers report their subjective evaluations after each run.

Here, the lane keeping performance is evaluated by two well-known indicators. The first one is the standard deviation of the lateral position (STDLP) which is related to visual distraction and cognitive workload [44]. A decrease of the STDLP indicates an improved driving performance. The second indicator is the root mean square error (RMSE) [45] which is computed as the root mean square of the lateral error. For subjective evaluation, all participants should evaluate the driving according to their feeling of *comfort*, *safety*, *control*, and *workload*, and should report it on a scale from 0 (worst) to 100 (best). Then, the Wilcoxon rank sum test is performed on the collected data to assess the significance of the results.

Since one driver did not perform the ST, his related data are excluded and only those of six other participants are used for the following analysis. The lane keeping performance results are reported in Fig. 20. On each whiskers box, the central mark is the median, and the edges of the box are the 25th and 75th percentiles.

Observe in Fig. 20 that in the first phase with attentive drivers (i.e., no ST condition), all indicators are similar for both manual and shared controls, and the Wilcoxon rank

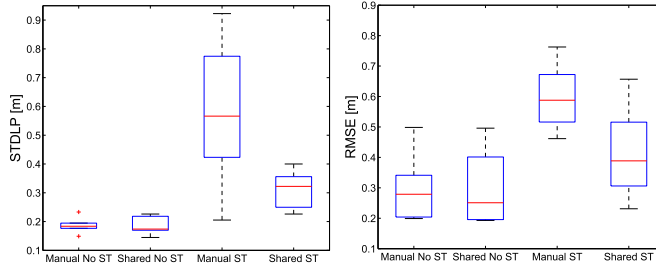


Fig. 20. Lane keeping performance: STDLP and RMSE.

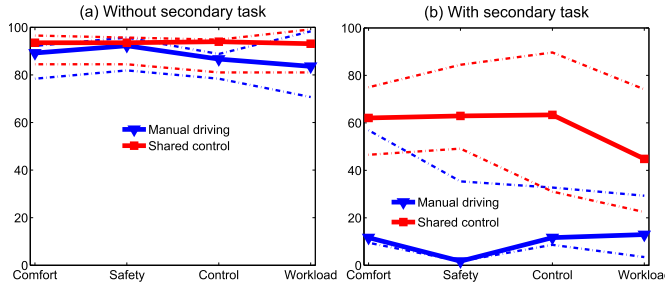


Fig. 21. Subjective assessment of the driving. (a) Driving without ST. (b) Driving while engaged in the secondary part.

sum test shows no significant difference. This means that when the drivers are attentive, the LKA system does not affect their driving behaviors. However, in the second phase with distracted drivers (i.e., the ST condition), the performance indicators show a clear improvement in the case of shared control. Indeed, the STDLP decreases significantly, with  $p$ -value = 0.033 for the Wilcoxon rank sum test, which means that there is less lateral position variability. In addition, the RMSE shows that the LKA system assists drivers to stay closer to the lane center than in the case of manual control (with  $p$ -value = 0.021).

Fig. 21 reports the subjective evaluation of driving according to the driver's feeling. Observe in Fig. 21(a) that for both the cases (manual and shared driving), when the drivers are attentive, their feeling of comfort, safety, control, and workload is quite similar. On the contrary, during the ST phase [see Fig. 21(b)], the participants' rating for the manual control dramatically decreases. The subjective results are improved in the case of shared control for all four considered criteria. The Wilcoxon rank sum test shows significant differences for three criteria: safety ( $p$ -value = 0.004), control ( $p$ -value = 0.047), and workload ( $p$ -value = 0.033). Moreover, all considered participants greatly appreciate the assistance provided by the LKA system, i.e., they fully have the authority to control the vehicle when they desire to drive, and they are smoothly assisted by the LKA system otherwise.

## VI. CONCLUSION

We have proposed a new cooperative control approach that can successfully share the driving control authority between human drivers and the LKA system. This control approach consists of a control supervisor (in the tactical level) and two local controllers with different driving objectives (in the operational level). The supervisor is in charge of decision-making

to manage the control authority between two driving actors according to the driver monitoring and the risk assessment. Both local controllers are designed by taking into account the knowledge of human behaviors. The outputs of these optimal-based controllers are weighted by a smooth authority transition signal given by the supervisor so that an appropriate assistance action can be computed for each specific driving situation. Using the Lyapunov stability argument in the LMI control framework, the closed-loop properties of the whole driver-vehicle system can be guaranteed.

Extensive experimental results obtained with human drivers and the SHERPA driving simulator have strongly demonstrated the effectiveness of the proposed shared control method. For future works, an *explicit* consideration of the vehicle speed variation in the control design is first investigated to improve further the robustness margins of the proposed shared control scheme. Then, a more realistic vehicle model taking into account the tire-road interaction through longitudinal and lateral wheel slip will be considered for the control design to deal with more aggressive maneuvers than the normal driving in highway conditions. Furthermore, despite promising results of the preliminary acceptability study, user test experiments will be explored more thoroughly in a wider experimental setup with the road test conditions.

## ACKNOWLEDGMENT

The authors would like to thank the anonymous reviewers and the Associate Editor for their valuable comments and suggestions to improve the quality of this paper.

## REFERENCES

- [1] J. Navarro, F. Mars, and M. S. Young, "Lateral control assistance in car driving: Classification, review and future prospects," *IET Intell. Transport Syst.*, vol. 5, no. 3, pp. 207–220, Sep. 2011.
- [2] NHTSA, "Visual-manual NHTSA driver distraction guidelines for in-vehicle electronic devices," Nat. Highway Traffic Safety Admin., Washington, DC, USA, Tech. Rep. NHTSA-2010-0053, 2010.
- [3] N. Enache, M. Netto, S. Mammar, and B. Lusetti, "Driver steering assistance for lane departure avoidance," *Control Eng. Pract.*, vol. 17, no. 6, pp. 642–651, Jun. 2009.
- [4] F.-Y. Wang, "Parallel control and management for intelligent transportation systems: Concepts, architectures, and applications," *IEEE Trans. Intell. Transp. Syst.*, vol. 11, no. 3, pp. 630–638, Sep. 2010.
- [5] L. Li, D. Wen, N.-N. Zheng, and L.-C. Shen, "Cognitive cars: A new frontier for ADAS research," *IEEE Trans. Intell. Transp. Syst.*, vol. 13, no. 1, pp. 395–407, Mar. 2012.
- [6] J. Wang, G. Zhang, R. Wang, S. C. Schnelle, and J. Wang, "A gain-scheduling driver assistance trajectory-following algorithm considering different driver steering characteristics," *IEEE Trans. Intell. Transp. Syst.*, vol. 18, no. 5, pp. 1097–1108, May 2017.
- [7] F. Flemisch, M. Heesen, T. Hesse, J. Kelsch, A. Schieben, and J. Beller, "Towards a dynamic balance between humans and automation: Authority, ability, responsibility and control in shared and cooperative control situations," *Cogn. Technol. Work*, vol. 14, no. 1, pp. 3–18, Mar. 2012.
- [8] L. Saleh, P. Chevrel, F. Claveau, J.-F. Lafay, and F. Mars, "Shared steering control between a driver and an automation: Stability in the presence of driver behavior uncertainty," *IEEE Trans. Intell. Transp. Syst.*, vol. 14, no. 2, pp. 974–983, Jun. 2013.
- [9] D. A. Abbink, M. Mulder, and E. R. Boer, "Haptic shared control: Smoothly shifting control authority?" *Cogn. Technol. Work*, vol. 14, no. 1, pp. 19–28, Nov. 2012.
- [10] A.-T. Nguyen, C. Sentouh, and J.-C. Popieul, "Driver-automation cooperative approach for shared steering control under multiple system constraints: Design and experiments," *IEEE Trans. Ind. Electron.*, vol. 64, no. 5, pp. 3819–3830, May 2017.

- [11] M. Shimakage, S. Satoh, K. Uenuma, and H. Mouri, "Design of lane-keeping control with steering torque input," *JSAE Rev.*, vol. 23, no. 3, pp. 317–323, Jul. 2002.
- [12] P. G. Griffiths and R. B. Gillespie, "Sharing control between humans and automation using haptic interface: Primary and secondary task performance benefits," *Hum. Factors*, vol. 47, no. 3, pp. 574–590, 2005.
- [13] M. Mulder, D. A. Abbink, and E. R. Boer, "Sharing control with haptics seamless driver support from manual to automatic control," *Hum. Factors*, vol. 54, no. 5, pp. 786–798, Oct. 2012.
- [14] M. Da Lio *et al.*, "Artificial co-drivers as a universal enabling technology for future intelligent vehicles and transportation systems," *IEEE Trans. Intell. Transp. Syst.*, vol. 16, no. 1, pp. 244–263, Feb. 2015.
- [15] J. E. Naranjo, C. Gonzalez, R. Garcia, T. de Pedro, and R. E. Haber, "Power-steering control architecture for automatic driving," *IEEE Trans. Intell. Transp. Syst.*, vol. 6, no. 4, pp. 406–415, Dec. 2005.
- [16] A.-T. Nguyen, C. Sentouh, and J.-C. Popieul, "Fuzzy steering control for autonomous vehicles under actuator saturation: Design and experiments," *J. Franklin Inst.*, to be published. [Online]. Available: <https://doi.org/10.1016/j.jfranklin.2017.11.027>
- [17] P. Falcone, F. Borrelli, J. Asgari, H. E. Tseng, and D. Hrovat, "Predictive active steering control for autonomous vehicle systems," *IEEE Trans. Control Syst. Technol.*, vol. 15, no. 3, pp. 566–580, May 2007.
- [18] T. Yang, "A new control framework of electric power steering system based on admittance control," *IEEE Trans. Control Syst. Technol.*, vol. 23, no. 2, pp. 762–769, Mar. 2015.
- [19] V. Cerone, M. Milanese, and D. Regruto, "Combined automatic lane-keeping and driver's steering through a 2-DOF control strategy," *IEEE Trans. Control Syst. Technol.*, vol. 17, no. 1, pp. 135–142, Jan. 2009.
- [20] X. Huang, H. Zhang, G. Zhang, and J. Wang, "Robust weighted gain-scheduling  $H_\infty$  vehicle lateral motion control with considerations of steering system backlash-type hysteresis," *IEEE Trans. Control Syst. Technol.*, vol. 22, no. 5, pp. 1740–1753, Sep. 2014.
- [21] A.-T. Nguyen, C. Sentouh, and J.-C. Popieul, "Sensor reduction for driver-automation shared steering control via an adaptive authority allocation strategy," *IEEE/ASME Trans. Mechatronics*, vol. 23, no. 1, pp. 5–16, Feb. 2018.
- [22] S. M. Erlien, S. Fujita, and J. C. Gerdes, "Shared steering control using safe envelopes for obstacle avoidance and vehicle stability," *IEEE Trans. Intell. Transp. Syst.*, vol. 17, no. 2, pp. 441–451, Feb. 2016.
- [23] J. Hespanha and A. Morse, "Switching between stabilizing controllers," *Automatica*, vol. 38, no. 11, pp. 1905–1917, Nov. 2002.
- [24] F. Vicente, Z. Huang, X. Xiong, F. D. L. Torre, W. Zhang, and D. Levi, "Driver gaze tracking and eyes off the road detection system," *IEEE Trans. Intell. Transp. Syst.*, vol. 16, no. 4, pp. 2014–2027, Aug. 2015.
- [25] Y. Dong, Z. Hu, K. Uchimura, and N. Murayama, "Driver inattention monitoring system for intelligent vehicles: A review," *IEEE Trans. Intell. Transp. Syst.*, vol. 12, no. 2, pp. 596–614, Dec. 2011.
- [26] S. Boyd, L. El Ghaoui, E. Feron, and V. Balakrishnan, *Linear Matrix Inequalities System Control Theory*, vol. 15. Philadelphia, PA, USA: SIAM, 1994.
- [27] R. Rajamani, *Vehicle Dynamic Control*. Boston, MA, USA: Springer, 2012.
- [28] E. Donges, "A two-level model of driver steering behavior," *Hum. Factors*, vol. 20, no. 6, pp. 691–707, Dec. 1978.
- [29] M. F. Land and D. N. Lee, "Where do we look when we steer," *Nature*, vol. 369, pp. 742–744, Jun. 1994.
- [30] D. D. Salvucci and R. Gray, "A two-point visual control model of steering," *Perception*, vol. 33, no. 10, pp. 1233–1248, Oct. 2004.
- [31] F. Mars, L. Saleh, P. Chevrel, F. Claveau, and J.-F. Lafay, "Modeling the visual and motor control of steering with an eye to shared-control automation," in *Proc. Hum. Fact. Ergonom. Soc. Annu. Meeting*, Sep. 2011, vol. 55, no. 1, pp. 1422–1426.
- [32] P. Hermannstädter and B. Yang, "Driver distraction assessment using driver modeling," in *Proc. IEEE Int. Conf. Syst., Man, Cybern.*, Manchester, U.K., Oct. 2013, pp. 3693–3698.
- [33] A. Ameyoe, P. Chevrel, E. Le-Carpentier, F. Mars, and H. Illy, "Identification of a linear parameter varying driver model for the detection of distraction," *IFAC-PapersOnLine*, vol. 48, no. 26, pp. 37–42, 2015.
- [34] C. Sentouh, P. Chevrel, F. Mars, and F. Claveau, "A sensorimotor driver model for steering control," in *Proc. IEEE Int. Conf. Syst., Man, Cybern.*, San Antonio, TX, USA, Oct. 2009, pp. 2462–2467.
- [35] S. Taheri, "Steering control characteristics of human driver coupled with an articulated commercial vehicle," Ph.D. dissertation, Dept. Mech. Eng., Concordia Univ., Montreal, QC, Canada, 2014.
- [36] L. Ljung, *System Identification*. Englewood Cliffs, NJ, USA: Prentice-Hall, 1999.
- [37] Z. Sun and S. Ge, "Analysis and synthesis of switched linear control systems," *Automatica*, vol. 41, no. 2, pp. 181–195, Feb. 2005.
- [38] J. Pohl, W. Birk, and L. Westervall, "A driver-distraction-based lane-keeping assistance system," *Proc. Inst. Mech. Eng. I, J. Syst. Control Eng.*, vol. 221, no. 4, pp. 541–552, Nov. 2007.
- [39] S. Glaser, S. Mammar, and C. Sentouh, "Integrated driver-vehicle-infrastructure road departure warning unit," *IEEE Trans. Veh. Technol.*, vol. 59, no. 6, pp. 2757–2771, Jul. 2010.
- [40] H. D. Tuan, P. Apkarian, T. Narikiyo, and Y. Yamamoto, "Parameterized linear matrix inequality techniques in fuzzy control system design," *IEEE Trans. Fuzzy Syst.*, vol. 9, no. 2, pp. 324–332, Apr. 2001.
- [41] J. Lofberg, "YALMIP: A toolbox for modeling and optimization in MATLAB," in *Proc. IEEE Int. Symp. Comput. Aided Control Syst. Design*, Sep. 2004, pp. 284–289.
- [42] G. J. Balas, J. C. Doyle, K. Glover, A. Packard, and R. Smith,  *$\mu$ -Analysis and Synthesis Toolbox: User's Guide*, The Mathworks, Natick, MA, USA, 1991.
- [43] L. Liu, M. Nagai, and P. Raksincharoensak, "On torque control of vehicle handling and steering feel for avoidance maneuver with electric power steering," *IFAC Proc. Volumes*, vol. 41, no. 2, pp. 12073–12078, 2008.
- [44] J. Östlund *et al.*, "Driving performance assessment-methods and metrics," Gothenburg, Sweden, Tech. Rep. IST-1-507674-IP, 2005.
- [45] K. K. Tsoi, M. Mulder, and D. A. Abbink, "Balancing safety and support: Changing lanes with a haptic lane-keeping support system," in *Proc. IEEE Int. Conf. Syst., Man, Cybern.*, Istanbul, Turkey, Oct. 2010, pp. 1236–1243.



**Chouki Sentouh** received the M.Sc. degree from the University of Versailles, Versailles, France, in 2003, and the Ph.D. degree in automatic control from the University of Évry, Évry, France, in 2007.

He was a Post-Doctoral Researcher with the Laboratory Institut de Recherche en Communications et Cybernétique de Nantes UMR CNRS 6597, France, from 2007 to 2009. Since 2009, he has been an Associate Professor with the Laboratoire d'Automatique, de Mécanique et d'Informatique industrielles et Humaines (LAMIH UMR CNRS 8201), University of Valenciennes, Valenciennes, France. His current research interests include automotive control, driver assistance systems with driver interaction, human driver modeling, and cooperation in intelligent transportation systems.



**Anh-Tu Nguyen** received the Engineering and M.Sc. degrees in automatic control from the Grenoble Institute of Technology, Grenoble, France, in 2009, and the Ph.D. degree in automatic control from the University of Valenciennes, Valenciennes, France, in 2013.

From 2014 to 2017, he was with the Laboratoire d'Automatique, de Mécanique et d'Informatique industrielles et Humaines (LAMIH UMR CNRS 8201), University of Valenciennes, and then with the Laboratory LS2N UMR CNRS 6004, Nantes, France. He is currently a Researcher with LAMIH UMR CNRS 8201, University of Valenciennes. His current research interests include robust control and observation, constrained systems, and human-machine-shared control with a strong emphasis on vehicle engineering applications.



**Mohamed Amir Benloucif** received the M.Sc. degree in electronic systems and robotics from the University of Versailles St-Quentin en Yvelines, Versailles, France, in 2013. He is currently pursuing the Ph.D. degree with the University of Valenciennes, Valenciennes, France.

His current research interests include automotive control, cooperation in intelligent transportation systems, and shared control for assistance systems.



**Jean-Christophe Popieul** received the Ph.D. degree in automatic control from the University of Valenciennes, Valenciennes, France, in 1994.

He is currently a Professor of automatic control with the Laboratoire d'Automatique, de Mécanique et d'Informatique industrielles et Humaines (LAMIH UMR CNRS 8201), University of Valenciennes. He is also the Head of several interactive simulation platforms of the Laboratoire d'Automatique, de Mécanique et d'Informatique industrielles et Humaines: the SHERPA driving simulator, the PSCHITT-Rail train/tramway simulator, and the PSCHITT-PMR wheelchair simulator. His current research interests include transport safety, driver status assessment, and shared control for full driving automation.

Dr. Popieul is a member of several scientific boards, including the Agence Nationale de la Recherche, PREDIT, i-Trans competitiveness cluster, and IRT Railenium.